



**KTH Chemical Science  
and Engineering**

# Solid Polymer Lithium-Ion Conducting Electrolytes for Structural Batteries

Markus Willgert

Doctoral Thesis

Kungliga Tekniska Högskolan, Stockholm 2014

AKADEMISK AVHANDLING

som med tillstånd av Kungliga Tekniska högskolan i Stockholm, framlägges till offentlig granskning för avläggande av teknisk doktorexamen fredagen den 25 april 2014, kl.14.00 i sal F3, Lindstedtsvägen 26, KTH, Stockholm. Avhandlingen försvaras på engelska. Fakultetsopponent: Professor Alexander Bismarck, University of Vienna, Austria.

Copyright © 2014 Markus Willgert  
All rights reserved

Paper I © 2011 European Polymer Journal  
Paper II © 2012 American Chemical Society  
Paper III © 2013 Solid State Ionics  
Paper IV Submitted Manuscript

TRITA-CHE Report 2014:7  
ISSN 1654-1081  
ISBN 978-91-7595-035-8

*To My Family*



# Abstract

This work comprises the manufacture and characterization of solid polymer lithium ion conducting electrolytes for structural batteries. In the study, polymer films are produced *in situ via* a rapid versatile UV irradiation polymerization route, in which ethylene oxide methacrylates are polymerized into thermoset networks. In the first part of the study, the simplicity and efficiency of this manufacturing route is emphasized. Polymer electrolytes are produced with an ionic conductivity ranging from  $5.8 \times 10^{-10}$  S cm<sup>-1</sup> up to  $1.5 \times 10^{-6}$  S cm<sup>-1</sup>, and a storage modulus of up to 2 GPa at 20°C. In the second part, the effect of the lithium salt content is studied, both for tightly crosslinked systems with a glass transition temperature ( $T_g$ ) above room temperature but also for sparsely crosslinked system with a  $T_g$  below. It is shown that for these systems, there is a threshold amount of 4% lithium salt by weight, above which the ion conducting ability is not affected to a larger extent when the salt content is increased further. It is also shown that the influence of the salt content on the ionic conductivity is similar within both systems. However, the  $T_g$  is more affected by the addition of lithium salt for the loosely crosslinked system, and since the  $T_g$  is the main affecting parameter of the conductivity, the salt content plays a larger role here. In the third part of the study, a thiol functional compound is added via thiol-ene chemistry to create thio-ether segments in the polymer network. This is done in order to expand the toolbox of possible building blocks usable in the design of structural electrolytes. It is shown that solid polymer electrolytes of more homogeneous networks with a narrower glass transition region can be produced this way, and that they have the ability to function as an electrolyte. Finally, the abilities of reinforcing the electrolytes by nano fibrillar cellulose are investigated, by means to improve the mechanical properties without decreasing the ionic conductivity at any larger extent. These composites show conductivity values close to  $10^{-4}$  S cm<sup>-1</sup> and a storage modulus around 400 MPa at 25 °C.

# Sammanfattning

Detta arbete innefattar tillverkning och analys av fasta litiumjonledande polymera elektrolyter för användning i strukturella batterier. I studien produceras polymerfilmer av etylenoxid-metakrylat in situ genom en snabb, mångsidig och effektiv tillverkningsmetod via UV-härdning. I den första delen av studien understryks enkelheten och effektiviteten hos denna tillverkningsmetod. Polymerelektrolyterna har en jonledningsförmåga som sträcker sig från  $5.8 \times 10^{-10} \text{ S cm}^{-1}$  upp till  $1.5 \times 10^{-6} \text{ S cm}^{-1}$ , och en lagringsmodul upp till 2 GPa vid 20°C. I del två undersöks egenskapsförändringarna hos de polymera elektrolyterna som funktion av andelen litiumsalt. Detta utförs både i ett system med hög tvärbindningsgrad med en glastransitionstemperatur ( $T_g$ ) över rumstemperatur, samt i ett system med låg tvärbindningsgrad med ett  $T_g$  under. Det visas att för båda systemen finns ett tröskelvärde när upp till 4 vikts-% salt är tillsatt över vilken ledningsförmågan inte påverkas nämnvärt. Det är även visat att influensen på jonledningsförmågan av salthalten följer samma trend inom respektive system. Däremot påverkas  $T_g$  mer av tillsats av litiumsalt i det system som är mindre tvärbundet, och eftersom  $T_g$  är den parameter som påverkar jonledningsförmågan mest så spelar salthalten större roll i detta system. I den tredje delen av studien tillsätts även monomer med tiol-funktionalitet genom tiolen-kemi för att skapa tio-etrar i det polymera nätverket. Detta är gjort för att utöka verktygslådan av möjliga byggstenar för konstruktion av polymera elektrolyter. Studien visar att mer homogena polymera nätverk med ett smalare glastransitionsområde kan skapas på detta sätt och att dessa polymera nätverk kan användas som solida elektrolyter. Slutligen undersöks möjligheterna att inkludera nanofibrillär cellulosa och på så sätt förstärka elektrolyterna mekaniskt utan att försämra jonledningsförmågan i någon större utsträckning. Hos dessa kompositer uppnås konduktivitetsvärden nära  $10^{-4} \text{ S cm}^{-1}$  och en lagringsmodul runt 400 MPa vid 25 °C.

# List of Publications

This thesis is a summary of the following articles and manuscripts, which are referred to in the text by Roman numerals and appended at the end of the thesis:

## Paper I (Published)

Photoinduced free radical polymerization of thermoset lithium battery electrolytes. Willgert, M.; Kjell, H, M.; Jacques, E.; Behm, M.; Lindbergh, G.; Johansson, M. *European Polymer Journal*, 2011 **47**(12), p. 2372-2378.

## Paper II (Published)

Effect of lithium salt content on the performance of thermoset lithium battery electrolytes. Willgert, M.; Kjell, H, M.; Johansson, M. In *Page, K., et al.; Polymers for energy storage and delivery: Polyelectrolytes for batteries and fuel cells*. ACS symposium series, Washington DC, 2012, pp. 55-65.

## Paper III (Published)

Thiol-ene systems in lithium ion conducting thermoset electrolytes. Willgert, M.; Kjell, H, M.; Lindbergh, G.; Johansson, M. *Solid State Ionics*, 2013 **236**, p. 22-29.

## Paper IV (Submitted manuscript)

Cellulose nanofibril reinforced composite electrolyte for lithium ion battery applications. Willgert, M.; Leijonmarck, S.; Lindbergh, G.; Malmström, E.; Johansson, M.

My contribution to the appended papers:

Paper **I**: All experimental work, DMA measurements, IR measurements, most of the preparation of the manuscript. EIS measurements and tensile testing were done in collaboration.

Paper **II**: All experimental work, DMA measurements, IR measurements. Most of the preparation of the manuscript. EIS measurements was done in collaboration.

Paper **III**: All experimental work and most of the manuscript preparations. All characterization except for EIS and sweep voltammetry which was done in collaboration.

Paper **IV**: All experimental work except preparation of the CNF gel. Most of the preparation of the manuscript. All characterization except for EIS and SEM which was done in collaboration.

Scientific contributions not included in this thesis:

Paper **V** (Published)

Surface-Grafted Conjugated Polymers for hybrid cellulose materials. Peterson, J, J.; Willgert, M.; Hansson, S.; Malmström, E.; Carter, R, K.; *Journal of Polymer Science Part A: Polymer Chemistry*, 2011 **49**, p. 3004-3013

Paper **VI** (Published)

Impact of electrochemical cycling on the tensile properties of carbon fibres for structural lithium-ion composite batteries. Jacques, E.; Kjell, H, M.; Zenkert, D.; Lindbergh, G.; Behm, M.; Willgert, M. *Composites Science and Technology*, 2012 **72**, p. 792-798

# Table of Contents

1. PURPOSE OF THE STUDY.....	1
2. INTRODUCTION.....	2
2.1. Lithium ion batteries .....	2
2.2. Structural batteries .....	4
2.3. Thermoset polymers.....	8
2.4. Free radical polymerization of acrylates/methacrylates.....	10
2.5. Free radical polymerization of thiol–ene systems.....	11
2.6. Fibre reinforcement in thermoset composites .....	12
2.6.1. Cellulose structures as reinforcement.....	13
2.7. Thermoset polymers and composites for structural .....	15
batteries .....	15
2.7.1. Chemistries.....	15
2.7.2. Processing.....	16
3. EXPERIMENTAL .....	20
3.1. Materials .....	20
3.1.1. General .....	20
3.1.2. Materials for preparation of CNF dispersions and CNF nanopapers....	21
3.1.3. Materials for modification of CNF nanopaper sheets.....	22
3.2 Procedure, single phase systems.....	23
3.3 Procedure, dual phase systems .....	24
3.3.1. Manufacturing of CNF-nanopaper .....	24
3.3.2 Acrylate and propionate modification of CNF nanopapers.....	25
3.3.3. Composite electrolyte preparation and photopolymerization.....	26
3.4. Techniques and Instrumentation .....	27
3.4.1. Electrical Impedance Spectroscopy (EIS), Paper I-III.....	27
3.4.2. Electrical Impedance Spectroscopy (EIS), Paper IV .....	28
3.4.3. Dynamical Mechanical Analysis (DMA).....	29

3.4.4. Tensile Testing.....	29
3.4.5. Fourier-Transform Infrared (FT-IR) and FT-Raman Spectroscopy .....	30
3.4.6. Density measurements.....	31
3.4.7. Field-Emission Scanning Electron Microscopy (FE-SEM).....	31
3.4.8. Sweep voltammetry.....	31
3.5 Experimental series.....	32
4. RESULTS AND DISCUSSION .....	<b>34</b>
4.1 General properties of the SPEs manufactured .....	37
4.2 Curing performance .....	37
4.3 Effect of crosslink density on the mechanical properties .....	41
4.4 Properties of ionic conductivity .....	49
4.5 Electrochemical stability .....	54
4.6 Swelling tests in EtOH.....	55
4.7 Composite electrolyte morphology.....	56
5. CONCLUSIONS .....	<b>57</b>
6. FUTURE WORK .....	<b>60</b>
7. ACKNOWLEDGEMENTS.....	<b>61</b>
8. REFERENCES .....	<b>64</b>

# 1. PURPOSE OF THE STUDY

The overall purpose of this study was to reveal details on the structure-property relationship for thermosets and thermoset composites acting as solid polymer electrolytes (SPEs) for structural lithium ion battery applications. The effects of crosslinking density, lithium salt content, as well as physical state of the polymer matrix have been studied. A study on the effect of coordination strength between the lithium ion and the polymer matrix has also been conducted using polymer networks containing thio-ethers in addition to traditional poly(ethylene oxide), (PEO), based networks. In the final study, cellulose nanofibrils (CNF) was used as a reinforcing phase in CNF/PEO composite in order to investigate the ability to take advantage of the mechanical properties of CNF as the load bearing component within a composite electrolyte. In all studies, the utilization of photo-induced polymerization is investigated as a versatile tool for rapid, robust *in situ* production of SPEs.

## 2. INTRODUCTION

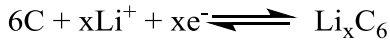
### 2.1. Lithium ion batteries

The development of batteries has been ongoing ever since the galvanic cell was introduced by Luigi Galvani in the late 1700's. Over the years to follow up to our days, persistent research has been carried out all over the world to improve the performance of battery cells. Numerous different elements have been investigated to create improved performance and functionality, such as for example increased cell voltage, shorter charging times. There are primary (non-rechargeable) and secondary (rechargeable) batteries. Interestingly enough, only three batteries (the primary  $\text{MnO}_2$  battery and the secondary lead/acid or nickel batteries) has been in use on a major scale over the last century [1]. However, relatively recent, new concepts have resulted in the lithium-ion battery, which has acquired significant attention due to its higher performance abilities. Among these abilities, its high energy density is of special importance, since this is of outermost significance as the continuous strive to store energy in small geometries proceeds.

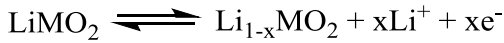
The lithium ion battery is in essence consisting of two electrodes, and a separating ion conducting membrane, or electrolyte (Figure 1). The electrodes generally consist of graphite (anode) and a lithium metal oxide or phosphate. Examples of such cathodes, with good reversibility for lithium intercalation/deintercalation, are lithium iron phosphate ( $\text{LiFePO}_4$ ) and lithium cobalt oxide ( $\text{LiCoO}_2$ ) which was developed and commercialized by Sony Inc. in 1991 [1].

Depicted below are the general redox reactions that occur in a lithium ion battery [2].

Negative electrode:



Positive electrode:



Total reaction



where  $\text{MO}_2$  is a metal oxide. In other words, during battery charge the lithium ions are transported from the positive to the negative electrode, accepting one electron and bond to the carbon. Accordingly, during discharge the ions will be transported back into the metal oxide, creating a current which can perform work.

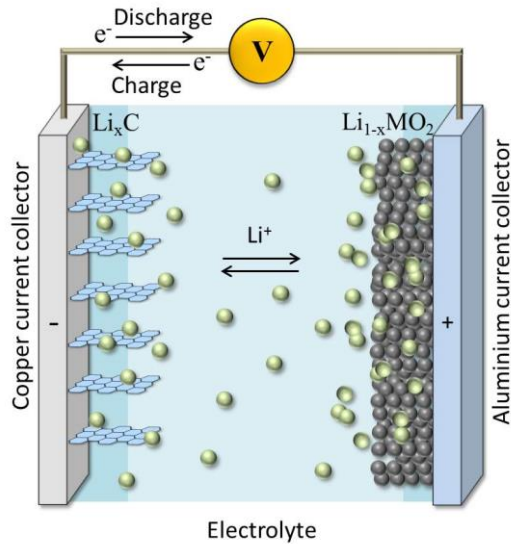


Figure 1. A generalized, schematic picture of the lithium ion battery.

A short circuit, i.e. when the two electrodes come in electrical contact, will result in battery malfunction or even more serious accidents. Therefore, the electrolyte must not only be the pathway for ions, but also be an electronic insulator, preventing the cell from short circuit.

The amount of lithium within the cathode is not sufficient for the cell to work. Therefore, additional lithium needs to be added to the electrolyte. This is normally done by dissolving a salt containing lithium in the electrolyte, where the most common ones are lithium hexa-fluoro phosphate ( $\text{LiPF}_6$ ), lithium triflate (lithium trifluoromethanesulfonate,  $\text{LiCF}_3\text{SO}_3$ ), and LiTFSI ( $\text{LiNCF}_3(\text{SO}_2)_2$ ). As can be seen, the difference between these three is the negative counter ion which will interact differently with the electrolyte [3]. Depending on the properties of the electrolyte to be used, different properties of the counter ion are desired [4].

## 2.2. Structural batteries

The concept of structural or multi-functional batteries was first introduced by Wetzel *et al.* in 2004 [5]. The concept originates from the desire of lowering the contribution of weight inflicted by the battery on the total weight of a portable electric device, by letting the battery be a part of the device construction and not only provide for the energy storage thus reducing the weight parasitic nature of the battery or capacitor [6]. The concept is suggested to resolve many of the challenges interlaced with the fact that the demands of energy storage is constantly increased as the devices are being more sophisticated, advanced and consume more energy. Examples of such electrical devices span from smartphones and laptops, but also electrical vehicles (EV) and hybrid electrical vehicles (HEV) can be included, where eve-

ry gram reduced from the weight results in a longer driving distance for a given battery charging period.

The basis for this concept is however in many parts connected to different earlier findings related to lithium ions in combination with polymers and the general concept of solid polymer electrolytes (SPE).

In 1966, Lundberg *et al.* presented strong evidences for the interaction occurring between alkali metal salts and PEO. They showed that the dilute solution viscosity of PEO was affected by addition of these salts, and that PEO with salt incorporated were soluble in methanol, whereas the neat polymer was practically insoluble [7]. Furthermore, they showed that the inclusion of salt strongly reduces the crystallinity of the material, and an elastomeric polymer is obtained. However, it was at that time not yet fully understood how this interaction occurred. The fact that alkali metal cations forms crystalline complexes with PEO was first presented by D. E. Fenton and P. V. Wright in the seventies [8, 9]. The cations studied were mainly potassium and sodium ions which were shown to coordinate to the electron lone pair of the ether oxygen. Each ion is able to coordinate to four ether oxygen simultaneously. They showed that the conductivity is largely dependent on the temperature at which the polymer is residing, and that it increases significantly when the degree of crystallinity of the polymer is decreased. It was also showed that the electric conductivity depends on the prevalence of amorphous regions in the polymer, which was later thoroughly investigated by Berthier *et al.* [10], and Shriver *et al.* [11], concluding that the amorphous (elastomeric) phase is governing the ionic conductivity at all temperatures. The mobility of the cations in these amorphous regions is also widely affecting the conductivity. This movement of cations is mainly restricted by the mobility of the polymer backbone of the PEO, which enables higher mobility of the ion when a large amplitude of the segmental motion of the polymer

is possible [12, 13]. This is why the amorphous regions are where the ion transport takes place, and hence why it is essential to minimize the crystalline regions throughout the SPE.

Further studies were conducted within the field, where not the least M. B. Armand and coworkers, but also others, have added substantial contribution in understanding the topic [14-18]. PEO is a highly crystalline polymer and one way to get around that, as showed by Killis *et al.* is to crosslink the polymer, thus making it to a thermoset and restricting the possibility of crystallization [19]. This action both decreases the proportion of crystalline regions, as well as increases the mechanical stability of the electrolyte. However, the mobility of the polymer becomes more restricted and ionic conductivity is reduced, why only a moderate degree of crosslinking can be accepted [16, 20]. One way to address this problem and push the performance of the electrolyte further is to create a heterogeneous two phase system, where one of the phases is acting as a reinforcing skeleton, allowing the other phase to be a flexible and soft component with a high ability to transport ions. There are many studies looking into the possibilities to take advantage of the concept of two-phase systems, where the usage employing fibres, inorganic particles, different types of inter penetrating networks (IPNs) and semi-inter penetrating networks (sIPNs) have been investigated [21-23], but also block copolymers prepared by atom transfer radical polymerization (ATRP) where the central block is ion conducting and the end blocks are crystallinity suppressing [24]. One reinforcing material that has gained augmented interest in the scope of electrode separators and electrolytes is cellulose fibrils or cellulose nanofibrils (CNF), either in composites structures [25-27], or as is, together with a liquid electrolyte [28]. Studies have also presented entire batteries with flexible characteristics constructed in CNF alone [29]. In Paper **IV** of this thesis, the usage of CNF nanopapers in composite electrolytes is explored, as one of the phases in a composite where the other phase is an ionic conductive polymer matrix. Earlier work has addressed difficulties associated with

phase migration when two phases of for instance different polarities are to be used in a composite [27, 30] . This also becomes critical if one of the phases is changing its geometry after manufacturing. In the scope of polymer or gel electrolytes, high ionic conductivity is mostly achieved through swelling of the polymer using a liquid electrolyte. It is known that neat polymer membranes may become very brittle and fragile upon swelling with a liquid electrolyte [26]. This behavior is vastly suppressed when reinforcing the membrane. Consequently, it is crucial to have a composite that does not deteriorate during the swelling process.

There are a number of advantages and possibilities using solid polymer electrolytes compared to liquid electrolytes of which a few follows:

i) Using a viscoelastic material in contact with a solid electrode is beneficial since it can lodge the volume changes of the electrode during intercalation. A material that holds such a property must be unordered on a molecular level and this also enables increased ion percolation in the material [14].

ii) Lithium ion batteries of today often contain liquid or semi-liquid electrolytes, where normally a lithium salt is dissolved in an organic solvent. Organic solvent liquid electrolytes are generally considered relatively unsafe and, if released or ignited, have a negative impact on people and/or the environment [31]. They are also typically quite harsh on the electrodes [32].

iii) If the use of organic solvents can be eliminated, or at least minimized, the electrolyte can hold quite the same mechanical properties as the neat polymer if one disregards the plasticizing effect of the salt. This opens up for a large number of possibilities, one of them being that the (battery) electrolyte can be used as a constructing material [5, 33-35].

The gain of this approach is quite obvious, namely to reduce the total weight of the material that needs to be carried (Figure 2). This way of approaching

the problem is, as mentioned above, applicable in a large number of mobile objects that require electrical energy, such as laptop computers, cellphones, electrical vehicles etc.



*Figure 2. Model car showing the principle of a structural battery; the roof is replaced by a laminate super capacitor which is able to run the lights of the car. (Printed with permission from Swerea SICOMP AB).*

### 2.3. Thermoset polymers

Thermoset polymers are polymer chains that have been chemically cross-linked. The fact that they are chemically crosslinked and not just physically “crosslinked” due to entanglements and secondary forces (like thermoplastics), makes them insoluble (Figure 3).

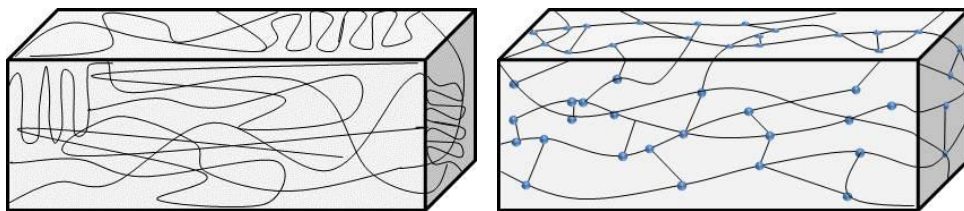


*Figure 3. Schematic picture of a semi-crystalline thermoplastic (left) and a crosslinked thermoset (right). The blue circles represent crosslinking sites.*

Furthermore, they are unable to melt upon heating [36], though if the temperature is high enough they will degrade [37]. If the crosslink density is relatively moderate it means that the molecular weight between the crosslinks is high. When this is the case, some polymers can therefore crystallize between the crosslinks, thus exhibiting some features associated with thermoplastics, such as the possession of a melting point [38]. Hence, if this is displayed in a thermal characterization it is due to physical changes in these regions, and shall not be interpreted as if the crosslinks are vanished. Thermosets have for long played an important role in material science when high or specific demands on the mechanical performance are needed for the final application. These polymers range from flexible, rubbery materials to stiff materials with excellent mechanical strength. It is well established that the final properties both depend on the physical structure, but also on the polymerization process and crosslinking mechanism utilized. A wide range of crosslinking chemistries are found, however they can in general be divided into two main mechanisms – step-wise or chain-wise reacting systems [39]. These polymerization reactions can furthermore be divided into sub-groups depending on the propagation mechanism where a main difference can be found between ionic or free radical mechanisms. The latter is by far the major mechanism used for production of commercial polymers due to its insensitivity to ionic / polar compounds, such as water that affect ionic systems. Most free radical propagating systems proceed via a chain-wise mechanism although ex-

emptions exists e.g. thiol-ene systems. The insensitivity toward ionic species during polymerization is one of the reasons why most systems employed as SPE materials are free radically polymerized acrylate systems, although work has been done using other crosslinking reactions such as for instance epoxide crosslinking or crosslinking of an isocyanate to form polyurethane [40, 41].

## 2.4. Free radical polymerization of acrylates/methacrylates.

Figure 4 shows a general reaction scheme for the free radical acrylate reaction mechanism. The reaction type is rapid and the propagation rate sometimes needs to be restricted by a retarding compound [42]. The reaction speed will also be lowered if methacrylates are used instead of acrylates. However, the reaction type is versatile and high molecular weights are achieved at low monomer conversions, on the contrary to step-wise polymerization [42]. If the proper initiator is used, the reaction can be initiated either by heat or by ultraviolet (UV) irradiation. The reaction is inhibited by the presence of oxygen, which enables peroxides of low reactivity to be formed at the surface. If this is the case, the material will exhibit a tacky and sticky surface due to unreacted monomer residues. Therefore, the polymerization should be performed in an inert atmosphere.

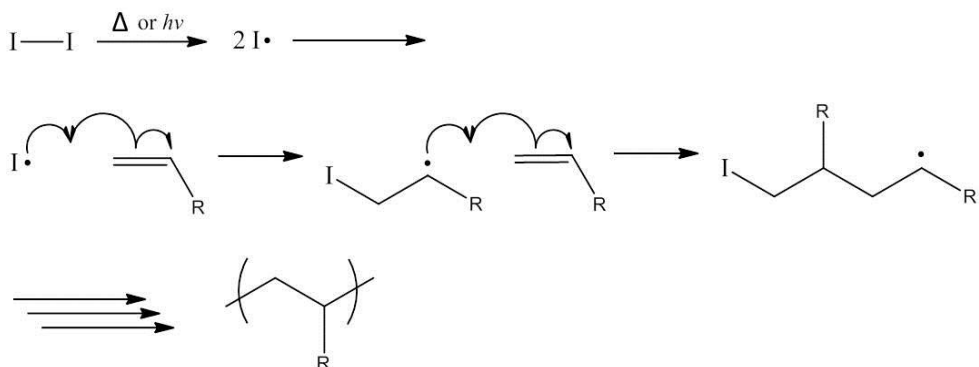


Figure 4. Generalized reaction scheme of the polymerization of an acrylate through a free radical mechanism, where I—I is the initiator.

## 2.5. Free radical polymerization of thiol–ene systems

A free radically polymerizing system that has obtained a renewed interest in the field of polymer science during the last decades is the so called “thiol–ene” system [43, 44]. Thiol–ene systems comprise of a combination of alkene and thiol monomers that can react radically to form thio–ether links between the monomers. A main difference to most other free radical polymerizations is that the reaction proceeds *via* a step–wise reaction mechanism (instead of chain–wise mechanism) [45], according to Figure 5. This is associated with a more homogeneous polymerization process and in the case of thermosets it is also related to a gel point at higher conversions, and therefore a more homogenous network is formed. It has earlier been shown that thiol compounds can be used as additives in for instance UV–cured poly(ethylene–oxide) membranes in polymerization reactions to high conversions [46]. On the account of drawbacks, the thiol–ene system suffers from bad odor and short shelf life. The thiol–ene system may also react spontaneously without an initiator being present [47].

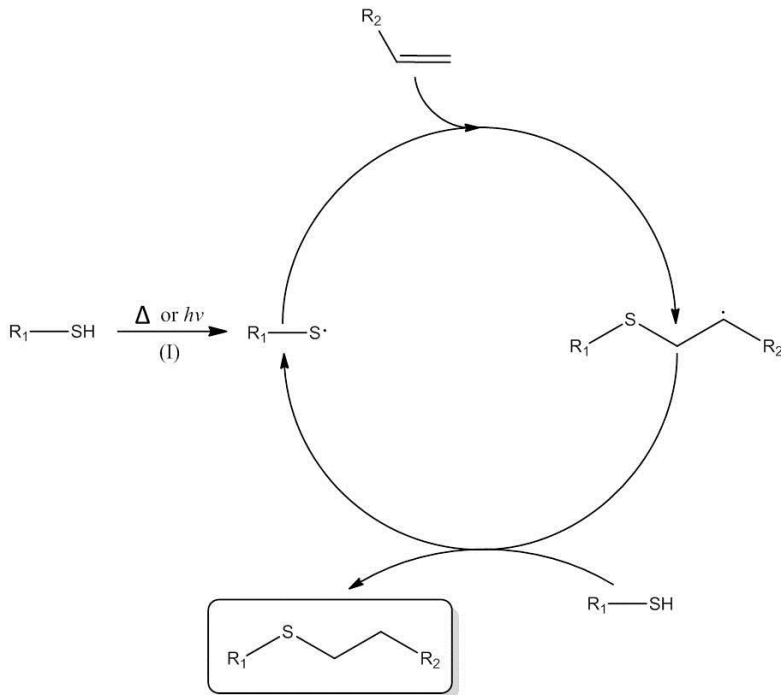


Figure 5. Generalized reaction scheme of the thiol-ene reaction.

## 2.6. Fibre reinforcement in thermoset composites

Thermoset composites can be reinforced using a number of different fibres ranging from glass fibres to carbon fibres, and natural fibres such as cellulose. The key parameters to optimize is the load bearing ability of the specific fibre type, interfacial interactions between the fibres and the matrix, orientation, size and shape of the fibres [48, 49]. Especially the size has during the last decades become a key parameter to address due to the introduction of nanosized reinforcements such as nano clays and nanofibres in so called nanocomposites. [23, 50-52] A decrease in fibre size increases surface area

and thus, the interfacial area between the fibres and the matrix with a subsequent increased importance of the interfacial properties. It has however been demonstrated that significant improvements of the properties can be obtained if nanosized fibres with the right interfacial properties are used. A specific reinforcement that has gained a significant interest lately in this respect is nanosized cellulose fibres and their use in composites [26, 53, 54].

### *2.6.1. Cellulose structures as reinforcement*

Cellulose is one of the most abundant natural polymer in the world and much work is carried out worldwide to find new applications in which the cellulose can be utilized [55]. There are numerous ways in which cellulose has been used and most of them involve some sort of modification or treatment for the application intended, since the often non-polar polymer matrix will be incompatible with the polar cellulose. There are many routes demonstrated for surface modification of the cellulose to create functional groups of which the matrix can react with, both physical treatment, as for instance physical adsorption or solvent exchange procedures, but also chemical modification. In many articles earlier presented regarding chemical modification of cellulose surfaces, the surface is modified with a small molecule, which can react with the hydroxyl group on the cellulose but also has another functional group compatible to the matrix. This creates a reactive center on the cellulose that can form a stable covalent bond between the phases, or be the initiator for a polymerization from the surface (i.e grafting) [30, 55-59].

On a molecular level cellulose consists of polymer chains having two anhydroglucose (AGU) rings in each repeating unit (Figure 6). These polymer chains are then gathered into cellulose nanofibrils i.e. CNF, that are aggregated in macroscopic fibres. The nanofibrils, which are consisting of both

amorphous and crystalline parts, are extracted from the fibres utilizing a homogenizing process, using high pressure which enables the CNF to be collected.

If the homogenizing process is not carried out but replaced with an acid hydrolysis process, cellulose nanocrystals (CNC), (generally referred to as cellulose whiskers) particles can be obtained [60]. In the scope of using CNC, of which the particles are shorter than in CNF, research has been conducted using modified CNC, in a number of applications, ranging from nanocomposites to bio-applications such as drug delivery systems and green catalysis [61-63]. Furthermore, bacterial cellulose have been used as the nanosized carbon source for electric capacitors [64].

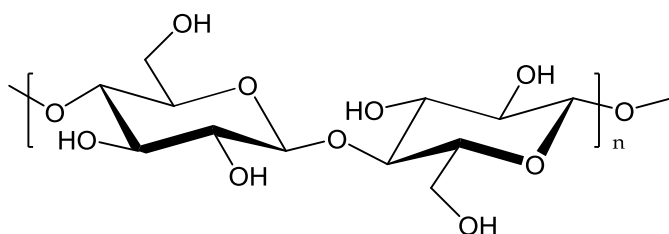


*Figure 6. The repeating unit of cellulose (two AGU) of the cellulose chain.*

The interesting features of CNF ranges from a high aspect ratio of the fibrils which makes it an interesting candidate as the reinforcing phase in a composite [53], to superior mechanical strength where values of the elastic modulus of single fibrils can reach as high as up to 140 GPa [65, 66]. The features of strength and the ability to form paper sheets having high porosity have highlighted this material for making strong, permeable membranes. Upon drying a slurry of a CNF dispersion, it forms a vast number of Van der Waals forces and hydrogen bonds between each fibril. The water extraction can take place for instance in a vacuum funnel, where the CNF slurry is poured onto a filter membrane with small pores, and the water is drawn out. When this residual water is drawn off, a CNF “cake” which subsequently can be dried in a vac-

uum oven is formed. Depending on the amount of the CNF present in the slurry that is poured onto the filter membrane, the thickness of this cake can be varied. As the water has left, the remaining CNF nanopaper will be dense, brittle and of low porosity. By the letting a solvent of lower polarity go through the CNF nanopaper cake, repelling forces will make it more porous and less brittle.

Aggregation and clogging is a large concern with untreated CNF fibres due to the large surface area in relation to volume (as for any nanosized particle). In order to decrease the fiber-fiber friction and hence the aggregation of the CNF, carboxylate groups can be developed through oxidation of the surface of the fibres through 2,2,6,6-tetramethylpiperidine-1-oxyl radical (TEMPO)-mediated oxidation [67, 68]. This increased charge density on the surface will decrease flocculation and the clogging tendency [69].

## 2.7. Thermoset polymers and composites for structural batteries

### 2.7.1. *Chemistries*

A number of different routes and polymers to produce thermoset SPEs have been evaluated in battery applications including poly(ether-urethane), to poly(propylene oxide), PEO/poly(acrylo nitrile), poly(organophosphazene), poly(siloxane) and also the use of plasticizers [41, 70-76]. The combination with a lithium salt in the final material has however restricted the number of possible candidates significantly. The aim has in most cases been to obtain a specific shape rather than a structural component. The pioneers in the field of structural batteries are D. E. Wetzal and

J. F. Snyder but also M.A Qidway, J.P Thomas and P. Liu *et al.* who have carried out a considerable amount of work in the field [5, 33-35, 77, 78]. In order to achieve better mechanical strength, work has been presented where for instance fibres are used as a reinforcement of the polymer matrix, but also other work presenting electrolytes reinforced on a molecular level by self-organization [79]. Other studies have also addressed the processing techniques in manufacture of these SPEs [80, 81] .

### 2.7.2. Processing

When using poly(ethylene-oxide) as ion transporting media it is, as aforementioned, important to suppress crystallization of the polymer which can be achieved through crosslinking the polymer. This is also in most cases needed in order to manufacture a load carrying mechanically robust polymer electrolyte. It is also important to incorporate the lithium salt in the polymer matrix for ion transport to occur. There are different routes in which these two things can be achieved with varied success which is described closer in the following sections.

#### 2.7.2.1. Thermally induced polymerization

Thermally induced polymerization is widely used in making thermosets and has shown to work also in the manufacturing of SPEs. Normally, the thermal initiator is dissolved in the monomer mixture and decomposed upon heating, forming active radicals. These radicals then attack the functional group on the monomer, for instance a methacrylate functionality or an acrylate functionality and the reaction propagate until termination occurs. The reaction mechanism is presented earlier in Figure 3, and heat is used to trigger the thermal initiator.

However, the method has a few drawbacks where the major one is that temperature gradients most likely will appear throughout the electrolyte upon heating. This will result in an earlier curing on the surface of the sample than inside, since the thermal initiator will get heated and decomposed at an earlier stage. Depending on what initiator is used, it may also result in that gas from the decomposing initiator is locked in the core of the sample, creating voids in the electrolyte. It is also possible that internal stresses will be built into the material due to this uneven cure rate. Consequently, the heating rate must be rather slow (to minimize heat gradients) and therefore the curing must take place over a long period of time, several hours and even up to days. Free radical polymerization of acrylates also generates a substantial amount of heat from the reaction itself which especially for larger geometries will affect the thermal load to the system.

#### 2.7.2.2. *Photo-induced polymerization*

An alternative to the thermal curing process is photo induced free radical polymerization techniques. This technique utilize UV-light instead of thermal energy to initiate the polymerization employing a photo initiator (in this study 2,2-dimethoxy-1,2-diphenylethanone (DMPA) is used, Figure 7) that decompose to free radicals under irradiation.

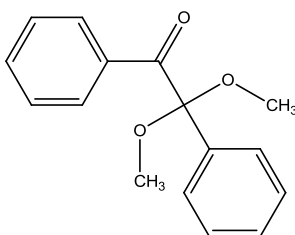


Figure 7. The photo initiator 2,2-dimethoxy-1,2-diphenylethanone (DMPA).

Several of the aforementioned drawbacks associated with thermal curing can be reduced or eliminated with this technique. Photo-induced polymerization is rapid, have low thermal impact, and well defined networks can be obtained, since initiation of the polymerization occurs simultaneously throughout the sample [82]. The technique is well established in several fields such as; coating technology [83] and dental composites [84], but now also in the scope of battery electrolytes [81, 85, 86]. Furthermore, this reaction mechanism proceeds, as for the thermal system, as presented above in Figure 3. One drawback of the method is that the mixture that is to be cured needs to be sufficiently transparent.

#### *2.7.2.3. Introduction of lithium salt into the system*

The addition of a lithium salt to the electrolyte is essential to make a functional electrolyte. There are a few different ways in which this can be actualized. A common route is to post swell the cured electrolyte gel in a lithium salt solution [86]. These solutions can be for instance lithium triflate or lithium hexafluorophosphate dissolved in for example ethyl carbonate (EC), diethyl carbonate (DEC), dimethyl carbonate (DMC) or a mixture of them. However, this approach is not very suitable for homogeneous polymer electrolytes in structural battery applications. Firstly, highly crosslinked thermosets must be used for mechanical strength which makes them restricted in their ability to swell and expand without cracking. Secondly, the introduction of a solvent strongly reduces the stiffness of the material, and finally it is challenging to ensure an even salt distribution throughout the electrolyte. Therefore, it is more applicable for structural electrolytes to add the lithium salt *in situ* by actually use the monomers as active diluents and dissolve the lithium salt directly in the monomer mixture, using the monomers as active diluents prior to cure [35, 77]. This can also be done using a proper solvent in the mixing step which later is evaporated prior to cure [87].

#### *2.7.2.4. Introducing reinforcements*

A vast number of techniques can be found with respect to introduction of reinforcements into thermoset composites. These range from filament winding of pre-soaked fibres to the use of pre-impregnated fibers finally formed to a composite under pressure. Important aspects for all these processes are to form a good wetting of the fibres and reduction of voids in the system as far as possible, since they give rise to stress concentrations and work as crack initiators in the composite [88].

## 3. EXPERIMENTAL

For the studies presented in this thesis, methacrylated PEO oligomers were chosen. Monomers used in the PEO thermoset polymer electrolytes in paper **I**, **II**, **III** and **IV** are oligomers with a number of repeating ethylene glycol units. Additionally, one of the studies performed (**III**) includes incorporation of thio-ethers to the structure; hence a thiol compound is used. All chemical structures are depicted in Figure 8.

### 3.1. Materials

#### *3.1.1. General*

The monomers/oligomers used in all studies are displayed in Figure 8. Tetraethylene glycol dimethacrylate (SR209)  $M = 330 \text{ g mol}^{-1}$ , and methoxy polyethylene glycol (350) monomethacrylate (SR550)  $M = 494 \text{ g mol}^{-1}$ , were kindly supplied by Sartomer Company, Europe. Trimethylol-propane-tri(3-mercaptopropionate) was kindly supplied by Bruno Bock Chemische Fabrik GmbH & Co (Germany). 2,2-dimethoxy-2-phenylaceto-phenone (DMPA) was thankfully received from Ciba Specialty Chemicals (Switzerland). Lithium trifluoromethanesulfonate (lithium triflate) 97% and lithium hexafluorophosphate ( $\text{LiPF}_6$ ) 97% was purchased from Chemtronica AB (Sweden). The photoinitiator used was 2,2-Dimethoxy-2-phenylaceto-phenone (Irgacure 651) was provided by Ciba Specialty Chemicals (Switzerland). For swelling of the CNF composite samples, a 1M solution of  $\text{LiPF}_6$  in ethyl carbonate (EC) and di-ethyl carbonate (DEC) (1:1 by volume) was prepared.

All reagents were used as received with no further purification, except for the lithium salts which were dried under vacuum at 80 °C for two days.

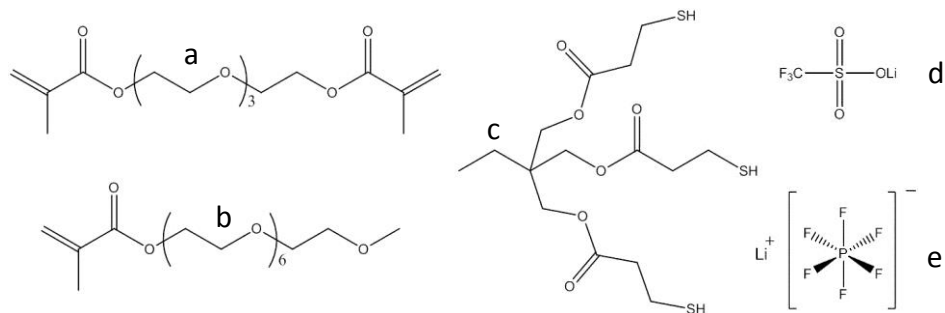


Figure 8. The di-methacrylate (SR209, (a)), the mono-methacrylate (SR550, (b)), and the thiol monomer (trimethylol-propane-tri(3-mercaptopropionate), (c)) as well as the lithium triflate salt (d) and the lithium hexafluorophosphate (e) used in these studies

### 3.1.2. Materials for preparation of CNF dispersions and CNF nanopapers.

A TEMPO oxidation was carried out on CNF fibrils according to the procedure described by Saito et al. [68]. First, the never-dried softwood dissolving pulp (40% Norwegian Spruce, 60% Scots Pine from Domsjö Fabriker AB, Örnsköldsvik, Sweden) was purified with 0.3% NaClO<sub>2</sub> in an acetate buffer (40 mL of acetate buffer per gram of dry pulp) at pH 4.6 and 60 °C, stirring for 1 h, followed by a washing step where the pulp was washed with deionized water through filtration. Thereafter, the pulp was re-dispersed in a phosphate buffer (90 mL of phosphate buffer per gram of dry pulp) at pH 6.8 and 60 °C. NaClO<sub>2</sub> (10 mmol, 80%), TEMPO (0.1 mmol) and NaClO (1.0 mmol) were calculated per gram of fiber and added to the flask where after the dispersion was stirred for 140 min at room temperature. At this

stage, the pulp was washed with deionized water through filtration. Finally, the charge density of the pulp was determined to be  $600 \mu\text{eq g}^{-1}$  by conductometric measurement as described by Katz *et al.* [89]. The pulp was then washed to convert the carboxyl groups to its sodium form before sheet preparation according to a procedure earlier described by Wågberg *et al.* [90]. After this pre-treatment, the fibres were homogenized using a high-pressure fluidizer (Microfluidizer M-110EH, Microfluidics Corp.) equipped with two chambers of different sizes connected in series (400 and 200  $\mu\text{m}$ ). The fibre suspension was passed three times in order to liberate the fibrils. This viscous suspension was then passed another three times through two pairs of chambers with dimensions 200 and 100  $\mu\text{m}$  respectively. Fully homogenization was achieved at a fibre concentration of 1 wt-% and an operating pressure of 1600 bar.

### 3.1.3. Materials for modification of CNF nanopaper sheets.

Acryloyl chloride  $\geq 97\%$  (**I**), propionyl chloride 98% (**II**), 4-(dimethylamino)pyridine (DMAP)  $\geq 99\%$ , dichloromethane (DCM)  $\geq 99.9\%$  and silicon dioxide ( $\text{SiO}_2$ ) 99.5%, 5-15 nm particle size were purchased from Sigma-Aldrich. **I** and **II** are shown in Figure 9. Ethanol (EtOH) 99% and 96% respectively, acetone  $\geq 99.5\%$  and n-pentane 99% were purchased from VWR International. Triethylamine (TEA)  $\geq 99\%$  and tetrahydrofuran (THF) 99.8% were purchased from Merck Millipore (Germany).

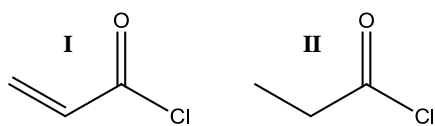


Figure 9. The acid chlorides used in modification of the CNF nanopaper in paper **IV**.

## 3.2 Procedure, single phase systems

Figure 10 shows the manufacturing route utilized in the work presented. The process is described in detail in Paper **I-III**. Monomers were mixed in vials in a glove box under inert, dry conditions and the lithium salt and the photo initiator were added to the mixture. The vials were then sealed and put on a shaking table overnight, allowing the lithium salt and photo initiator to dissolve completely. When applicable, the thiol monomer was added and the mixture was stirred until the compounds were completely mixed until no phase separation was present. At this stage, 0.3 ml of each sample solution was transferred into a Teflon mold using a syringe. Finally, the solution was cured for 4 minutes under UV irradiation at ambient temperature. The SPEs obtained were transparent and smooth. After curing, the products were taken out of the molds and cut into pieces of appropriate size, for further characterization.



sheet was then subjected to a solvent exchange procedure, where different solvents were subsequently poured over and passed through the sheet as following: 50 mL EtOH (96 %), 50 mL EtOH (99 %), 50 mL dry acetone and finally 50 mL pentane. The CNF sheet was never allowed to dry between additions of the different solvents, except for in the first step when the water was passed through prior the addition of EtOH. Once the pentane had passed the filter, the CNF sheet was peeled off from the filter and dried under vacuum at 110 °C overnight in a P Selecta Buch & Holm Vacuo-temp vacuum oven.

### *3.3.2 Acrylate and propionate modification of CNF nanopapers*

Pieces (1 cm<sup>2</sup>) of CNF were cut from the same CNF sheet produced and put in an Erlenmeyer-flask. The samples were then carefully washed with EtOH, acetone, THF and pentane. The samples were ultrasonicated for 2 minutes in each solvent (10 mL), and dried in a MMM VACUCELL vacuum oven for 12 hours at 55 °C. Each sample piece was put in separate vials, and DCM (10 mL) was added, followed by a catalytic amount of DMAP, TEA (34 µL (0.24 mmol)). Finally was a mixture of acryloyl chloride/propionyl chloride added drop wise to samples A-C in the ratios presented in table 1. No acid chlorides were added to the vials containing the reference samples (Ref1,2), which apart from this step were treated identical to the other samples. The reaction mixture was put on a shaking table and left to react overnight. After the reaction, the solution was poured off and the modified and unmodified pieces of CNF was washed thoroughly with EtOH, THF, DCM and pentane, and sonicated in each solvent for 2 minutes. Finally, the samples were once again dried in a vacuum oven for 12 hours at 55 °C.

Table 1. Details of modification solutions used in Paper **IV**<sup>a,b</sup>

Sample name \ Acid chloride	Acryloyl chloride ( <b>I</b> )	Propionyl chloride ( <b>II</b> )	Stoichiometry ( <b>I:II</b> )
Ref1, Ref2	-	-	0:0
A1, A2	(0.2 mmol)	(2 mmol)	1:9
B1, B2	(2 mmol)	(0.2 mmol)	9:1
C1, C2	(1.1 mmol)	(1.1 mmol)	1:1

<sup>a</sup>All sample vials contained 34 $\mu$ L (0.24 mmol) TEA

<sup>b</sup>All sample vials contained a catalytic amount of DMAP

### 3.3.3. Composite electrolyte preparation and photopolymerization

The following general procedure was used for the preparation and curing of the polymer electrolyte composite membranes. The PEO oligomers (5 wt-% of **a** and 95 wt-% of **b**) were mixed in vials in a glove box under dry conditions, (<1 ppm H<sub>2</sub>O), under argon. The dried lithium salt (8 wt-% of the total oligomer weight) and the photo initiator (2 wt-% of the total oligomer weight) were added to dissolve in the mixture. The vials were then sealed and placed on a shaking table overnight, allowing the lithium salt and the photo initiator to dissolve completely.

The modified and unmodified CNF nanopaper pieces were immersed in a vial containing the monomer mixture, and the vial was connected to a vacuum/argon line. Vacuum was then applied until no bubbles were observed, and the paper appearance had turned from white to transparent.

At that moment, argon was allowed to enter the vial increasing the pressure back to normal atmospheric pressure. This cycle was performed for three times to allow complete removal of entrapped air as well as oxygen present in the system. When this was accomplished, the vial containing the monomer mixture as well as the CNF nanopaper was taken inside the glove box. The wet CNF nanopaper was removed from the mixture and put between

two polyester plastic films (Mylar®). Finally, a microscope lab glass slide was put on top and the sample was irradiated for 10 minutes on one side + 3 minutes on the other under UV irradiation at 15 cm distance from the UV light source, and the resulting, fully cured, still transparent composite electrolyte film was peeled off the Mylar® films. The temperature of the sample did not exceed 42 °C during cure. The light source used for curing was a Blak Ray B-100AP (100 W, 365 nm) Hg UV lamp, which after the aforementioned irradiation time subject the sample to a total dose of 4.1 J cm<sup>-2</sup>, as determined using an Uvicure Plus High Energy UV Intergrating Radiometer (EIT, USA), measuring UVA at 320-390 nm. After irradiation, the composite electrolyte was swollen in EC:DEC (1:1) for 2 hours, after which the different characterizations were conducted. Additionally, two neat polymer reference samples without any CNF nanopaper were manufactured. One of them was characterized as is and one was swollen as described above before characterization.

### 3.4. Techniques and Instrumentation

#### *3.4.1. Electrical Impedance Spectroscopy (EIS), Paper I-III*

The electrochemical performance of the SPEs were quantified using a four-electrode test cell, consisting of four gold wires (two working electrodes with 20 mm distance and two reference electrodes, 5 mm distance) and two Plexiglas plates with screws to hold the sample (15×20×1 mm) in place. The impedance was potentiostatically measured in the frequency range 1 Hz to 300 kHz, at 10 points per decade using an amplitude of 10 mV. The instrument utilized was a Gamry Series G 750 Potentiostat/Galvanostat/ZRA interface, in an argon atmosphered glove box (<0.05 ppm H<sub>2</sub>O) at ambient temperature.

### 3.4.2. Electrical Impedance Spectroscopy (EIS), Paper IV

The electrochemical performances of the composite electrolytes were quantified using a two-electrode test cell, consisting of two stainless steel block electrodes in which between two copper gauge blocks (6.5×6.5×1 mm) and the sample (10×10×0.15 mm) was mounted (Figure 11). The copper blocks were used in order to ensure the measurements were actually taking place through the composite electrolyte, and not through excess polymer matrix on the edges and/or liquid electrolyte. The impedance was measured around open circuit potential (OCP) in the frequency range 0.1 Hz to 300 kHz, at 10 points per decade using an amplitude of 10 mV. The instrument utilized was a Gamry Series G 750 Potentiostat/Galvanostat/ZRA interface, in an argon-filled glove box (<1 ppm H<sub>2</sub>O) at 25 °C.

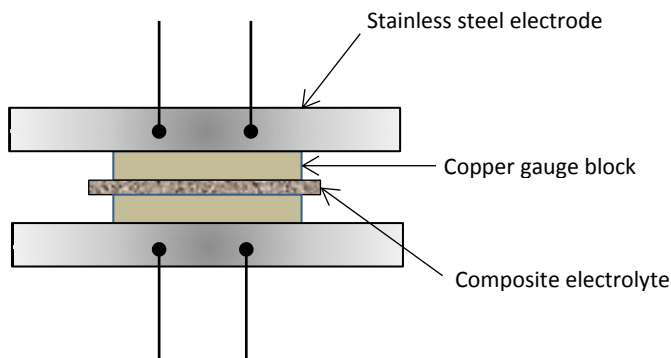


Figure 11. A schematic figure of the EIS setup.

### 3.4.3. Dynamical Mechanical Analysis (DMA)

Dynamical mechanical analysis (DMA) tests were performed on a TA instruments DMA, model Q800 in tensile mode. Samples pieces were cut from the initial sample pieces from the curing so they possessed geometry of  $7\times 5\times 1$  mm in Paper **I-III** and  $5\times 20\times 0.15$  mm in Paper **IV**. The specimens were tightened in the clamps of the sample holder, and the temperature was decreased to, and held at, the starting temperature ( $-60$  °C) for 5 minutes before the measurements were started. The temperature was then increased by  $5$  °C  $\text{min}^{-1}$  up to a final temperature of a sufficient magnitude where the glass transition temperature,  $T_g$ , is passed by as data was recorded. The oscillation frequency was held at 1 Hz at constant amplitude of  $10.0$   $\mu\text{m}$ . DMA measurements gave values for storage modulus ( $E'$  both at  $20$  °C and in the rubber plateau region), loss modulus ( $E''$ ), loss factor ( $\tan \delta$ ) and  $T_g$  for the electrolytes.

### 3.4.4. Tensile Testing

Uniaxial tensile tests were performed (Paper **I**) inside a glove box under argon atmosphere using a tensile stage from Deben UK equipped with a 10 mm maximum extensometer and a 300 N load cell. Dumbbell-shaped specimens were manufactured with an initial length of 10 mm and an average cross section area of  $3.3$   $\text{mm}^2$  ( $1.02\times 3.28$  mm). The samples were pulled at a total rate of  $0.2$  mm/min, providing a strain rate of  $2.7\times 10^{-6}$   $\text{s}^{-1}$ . This strain rate is  $< 10^{-5}$   $\text{s}^{-1}$ , which is the rate limit above which the motor speed is assumed to affect the results. The initial cross section area of the sample is considered to be constant, and data were recorded and plotted as stress ( $\sigma$ ) vs. strain ( $\epsilon$ ) to obtain stress at break ( $\sigma_b$ ), elongation at break, ( $\epsilon_b$ ) and Young's modulus.

### 3.4.5. *Fourier-Transform Infrared (FT-IR) and FT-Raman Spectroscopy*

All samples were characterized with FT-IR prior to and after modification, to verify the presence of acrylate and propionate groups. Furthermore, the composite electrolyte samples were also characterized after curing to make sure the composites were sufficiently cured. All FT-IR analysis was performed using a Perkin-Elmer Spectrum 2000 FT-IR instrument (Norwalk, CT) equipped with a single reflection (ATR: attenuated total reflection) accessory unit having a diamond ATR crystal (Golden Gate) from Graseby Specac Ltd. (Kent, England). The penetration depth is circa 1-5  $\mu\text{m}$  depending on the wavenumber. Spectrum software was utilized to evaluate the data. All IR measurements were performed in reflection mode, with a resolution of 4  $\text{cm}^{-1}$ .

In Paper **I-III**, the disappearance of the vinyl stretch peak at 1637  $\text{cm}^{-1}$  was confirmed after 4 minutes of UV irradiation. Furthermore, FT-Raman measurements were carried out in Paper **III** using a Perkin-Elmer Spectrum 2000 NIR-Raman equipment with Spectrum software to monitor the prevalence of pendant thiol groups at 2575  $\text{cm}^{-1}$  remaining in the crosslinked thiol-ene electrolyte films. Each spectrum collected was based on 16 scans using a laser power of 1000 mW.

In Paper **IV**, free standing composite electrolyte films were obtained by peeling off from the Mylar® films and mounted onto the instrument, with the bottom side of the sample (exposed to 3 minutes of irradiation) facing the crystal. The disappearance of the vinyl stretch peak at 1637  $\text{cm}^{-1}$  was confirmed after 10 + 3 minutes of UV irradiation. Each spectrum was based on 32 scans.

#### *3.4.6. Density measurements*

In order to determine the average molecular weight between crosslinks ( $\bar{M}_c$ ) in Paper **III**, the density was measured with a Mettler Toledo Precisa XR 20SSM-DR kit utilizing Archimedes principle to obtain the specific density of each sample. Each measurement was conducted three times, using heptane as auxiliary liquid at ambient temperature.

#### *3.4.7. Field-Emission Scanning Electron Microscopy (FE-SEM)*

The fracture surfaces of the cured composite electrolytes were examined by SEM using a Hitachi S-4800 equipped with a cold field-emission electron source. Images were captured for samples Ref, A and B to examine the coverage of the polymer in the CNF nanopapers. The samples were cut using a scalpel through the composite electrolyte. The fracture surfaces of all samples were coated with Pt/Pd using Agar HR sputter coaters and the sputtered layers were around 5 nm thick.

#### *3.4.8 Sweep voltammetry*

For the sweep voltammetry measurements, two samples from series 3.1-3.5 were prepared. One containing no thio-ethers (3.1) and one with 20 wt-% thiol compound (3.5) with respect to monomers **a** and **b** (Figure 8). Samples from the least crosslinked series was chosen, since a too high resistance of the more cross-linked series may influence on the measurement. Furthermore, it is more likely that chemical reactions will occur at a larger extent in a flexible electrolyte than in a stiff one.

The experiments were carried out at a sweep rate of 1 mV/s, and the software was recording data each second. The anodic sweep measurement was performed from the open circuit potential (OCP) and 6 V vs. Li/Li<sup>+</sup>, and the cathodic sweep was conducted from OCP to 1 mV vs. Li/Li<sup>+</sup>.

### 3.5 Experimental series

In order to establish the results presented in Paper **I-III**, a number of test series were prepared (Table 2). There are three different studies performed and they are noted as **I**, **II**, and **III** according to the corresponding Paper.

Table 2. presentation of the test series prepared.<sup>a</sup>

Sample name	SR209	SR550	Thiol	Li-salt	
1.1	5	95	-	12	I
1.2	10	90	-	12	
1.3	20	80	-	12	
1.4	30	70	-	12	
1.5	40	60	-	12	
1.6	50	50	-	12	
1.7	60	40	-	12	
1.8	70	30	-	12	
1.9	80	20	-	12	
1.10	50	50	-	6	
1.11	50	50	-	9	
(1.6)	50	50	-	12	
1.12	50	50	-	15	
1.13	50	50	-	18	
2.1	20	80	-	0	II
2.2	20	80	-	2	
2.3	20	80	-	4	
2.4	20	80	-	8	
2.5	20	80	-	12	
2.6	20	80	-	16	
2.7	50	50	-	0	
2.8	50	50	-	2	
2.9	50	50	-	4	
2.10	50	50	-	8	
2.11	50	50	-	12	
2.12	50	50	-	16	
3.1	40	60	-	8	III
3.2	40	60	5	8	
3.3	40	60	10	8	
3.4	40	60	15	8	
3.5	40	60	20	8	
3.6	60	40	-	8	
3.7	60	40	5	8	
3.8	60	40	10	8	
3.9	60	40	15	8	
3.10	60	40	20	8	
3.11	80	20	-	8	
3.12	80	20	5	8	
3.13	80	20	10	8	
3.14	80	20	15	8	
3.15	80	20	20	8	

<sup>a</sup> The numbers given in the table are in weight percent of SR209+SR550, except for the lithium salt which is in weight percent of SR209+SR550+thiol.

## 4. RESULTS AND DISCUSSION

For the studies presented in this thesis, methacrylated PEO oligomers were used. The specific oligomers used in the thermoset polymer electrolytes in Paper **I-IV** are, as described above, oligomers with a number of repeating glycol units.

The monomers need to have at least one functional group in order to polymerize, or two (or more) if the monomer is supposed to work as a crosslinker. In this study, di-methacrylated PEO is used as a crosslinker (for mechanical robustness), and mono-methacrylated PEO is used as a softener that provides ionic conductivity. The relative amount at which they are used will affect these two properties. The mono-methacrylate will create dangling chain ends and the di-methacrylate will crosslink the polymer, forming the polymer network. Paper **I** described PEO systems towards structural battery applications. It emphasized the large influence of the physical state in which the polymer was residing, and had a heavy focus on the processing technique utilized to manufacture the SPEs. Since it was possible to use the monomers as active diluents, the lithium salt could be dissolved directly in the monomer mixture, and no solvent was needed. In Paper **II** the same oligomers as in Paper **I** was used, although the focus was directed towards the influence of lithium salt content on the mechanical and ion conducting properties, at different crosslinking densities (and hence different  $T_g$ s of the thermoset)

As mentioned above, in the third Paper a thiol compound is added to the group of monomers used in designing the SPEs to incorporate thio-ethers in the structure. This is done in order to meet the demands and conditions reigning in the work of designing SPEs, where it is important to investigate novel routes in which SPEs can be realized. The aim of the study presented in Paper **III**, was firstly to reveal if thiol-ene chemistry could be performed in the presence of a lithium salt and secondly how the incorporation of thio-

ether links affects the performance of material as a structural electrolyte. Introduction of thio-ethers might have an interesting influence on both the mechanical properties as well as on the ion conducting ability of the SPE. Introduction of sulfur to the polymer network may result in a looser overall coordination strength to the lithium ion, since the interaction between sulfur and a lithium ion is weaker than the interaction between oxygen and lithium [91], thus improving the ionic conductivity at a lower cost of mechanical performance.

Finally Paper **IV** addresses the aforementioned issue of phase separation via a post functionalization of the fibril surfaces to enhance the interfacial strength in the final composite membrane. As earlier mentioned, there are limitations on how high the mechanical performance can be without paying a too high of a price in ionic conductivity in a thermoset polymer electrolyte. In many cases this is not necessarily an immense problem, since the entire cell is mechanically supported by a surrounding case of which the mechanical properties are dependent. This is however not the case in a structural battery, where all participating components needs to manifest mechanical integrity. Therefore, it is wishful to complement a soft, flexible ion conducting media with a load bearing reinforce which in this case is CNF.

There are different ways in which the reinforcing CNF can be added to the system. Herein, work has been conducted where the fibres are simply dispersed in a monomer/oligomer solution with subsequent cure of the system [25].

In this work, the CNF nanopaper is modified through an acid chloride reaction to create acrylate and alkyl groups on the surface, where the acrylate can react with a PEO-methacrylate to create covalent bonds between the two,

and the alkyl can work as a “dummy”, to lower the extent at which OH-groups of the CNF interact with the PEO.

However, in the first step of the work described in this thesis, a porous CNF nanopaper has been manufactured and dried. Secondly, the CNF nanopaper is immersed into a vessel containing an oligomer mixture, which is prepared with lithium salt as the *in situ* route described in section 2.7.2.3. At this stage, vacuum is created in the vessel and the air inside the pores of the CNF is replaced with oligomer solution. When no air bubbles are emitted from the CNF nanopaper anymore, argon gas is applied and by this, one cycle is accomplished. This cycle is conducted three times, making the CNF nanopaper go from white to transparent due to the change in refractive index as the air leaves, Figure 12. From this procedure a wet, transparent CNF nanopaper filled with oligomer solution having both the lithium salt and the photo initiator dissolved is obtained, and the material is cured into a composite electrolyte in an oxygen free environment (to prevent oxygen inhibition) into a composite electrolyte.

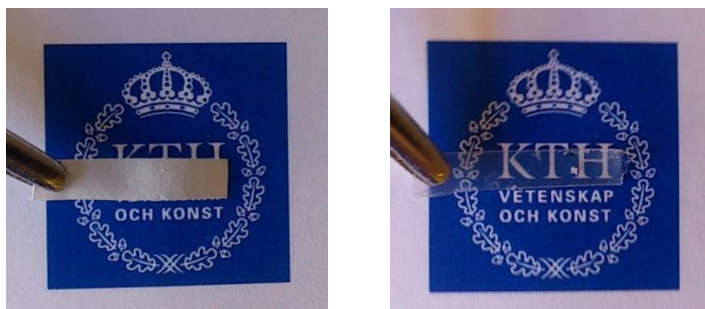


*Figure 12. The CNF nanopaper is opaque (left). After removing the entrapped air the paper becomes transparent (right).*

## 4.1 General properties of the SPEs manufactured

In Papers **I-III** the tremendous influence of crosslink density on most properties of the SPEs was demonstrated in electrical impedance spectroscopy and dynamic mechanical analysis, but also in uniaxial tensile tests. However all specimens, also in Paper **IV** were smooth, non-sticky, transparent films that were easily ejected from the Teflon mold or peeled of the Mylar® film respectively, and easy to handle for further characterization. The films with the largest amount of the thiol compound exhibited a tendency to be brittle to some extent, while the rest of the films did not cause any difficulties to characterize.

## 4.2 Curing performance

The SPEs and composite electrolytes were manufactured utilizing photo induced UV irradiation polymerization, and the method was shown to hold large advantages i.e. the method showed to be a rapid, robust processing technique suitable for the application, and in Paper **I-III** a degree of cure >91% was obtained after 4 minutes, except for some of the samples with high thiol compound content in Paper **III**. The composite electrolytes in Paper **IV** were cured for 10 + 3 minutes, also this resulting in a fully cured material. The samples were never subjected to a higher temperature than 42°C upon cure, which is a large advantage comparing to thermal initiation. The manufacturing route offers the ability to add the lithium salt in situ and as a result smooth, freestanding films were readily made.

Studies showed that the lithium salt did not hinder the SPEs from getting fully cured. The curing reaction of methacrylates did swiftly yield high monomer conversions. When the mixtures in Paper **I-III** had been irradiated for 4 minutes, and received an irradiation dose of  $1.25 \text{ J cm}^{-2}$ , FT-IR measure-

ments on the material showed a conversion of the vinyl bond (at  $\sim 1640\text{ cm}^{-1}$  and  $\sim 815\text{ cm}^{-1}$ ) in the methacrylate group higher than 91%, regardless of the presence of lithium salt. In the case of the composite electrolytes (Paper **IV**), a total dose of  $4.1\text{ J cm}^{-2}$  was imposed. Figure 13 shows the conversion of the methacrylate group during polymerization. One curve corresponds to sample 1.6 and the other to sample 1.6 with no lithium salt present. As can be seen, the conversion for sample 1.6 with salt is slower, which is proposed to be due to diluting effects of the salt. However, also this sample is fully cured after 4 minutes.

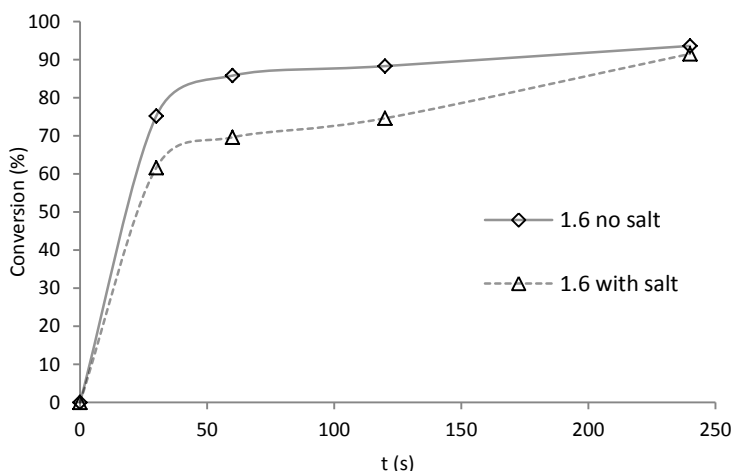


Figure 13. FT-IR results depicted as conversion of the vinyl bond in the methacrylate group (at  $1637\text{ cm}^{-1}$ ) vs. irradiation time. The lines should only be regarded as trend lines.

For the study including the thiol compound (Paper **III**) it was shown in FT-IR measurements that the peak stemming from the vinyl bond in the methacrylate also here was completely vanished after 4 minutes of UV irradiation (Figure 14a). Results from FT-Raman shows that the peak corresponding to the thiol group had completely disappeared after this time for the sample with 5% thiol, sample 3.2 (Figure 14b) and the material was thus fully cured.

On the other hand the measurement also showed that residual thiol groups were present after cure for the sample with the largest portion of thiol, (sample 3.5), (Figure 14b). The FT-Raman measurement was repeated for a sample containing no lithium salt but the same proportion of thiol, and the thiol corresponding peak was gone (Figure 14c).

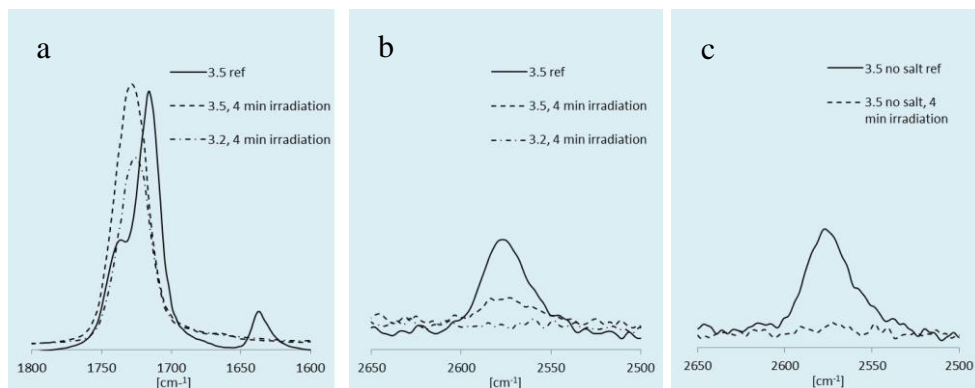


Figure 14. Enlargement in spectra from a) FT-IR measurements to monitor the disappearance of the peak corresponding to the methacrylate vinyl bond and b) and c) FT-Raman measurements to determine the prevalence of unreacted thiol groups.

These results indicate that the lithium salt interacts with the propagating thiyl radical and retard the addition to the methacrylate double bond. The propagation of the thiol–ene reaction is normally more rapid than the homopolymerization of methacrylates which is also seen in the test without any lithium salt present. Since there is a complete conversion of the methacrylate double bonds this indicate that the lithium salt interacts more strongly with the thiyl radical compared to the carbon centered radical on the methacrylate. The exact mechanism of this interaction is however not fully understood and further studies are needed to disclose details on this interaction. Nonetheless, the amount of remaining thiol is however low which can be seen on the high noise level in the spectra. This furthermore means that the results merely should be interpreted as an indication of an interference of the

lithium salt. The event of having residual thiol groups will result in a larger portion of free volume in the SPE, and this will also affect the modulus of the SPE and make it softer. However, the electrolyte is a clear, transparent thermoset even when thio-ethers are present in the system, and the lithium triflate salt shows no inclinations of aggregation, but is completely dissolved.

As described above and in earlier studies the UV curing method works well for manufacturing of PEO-methacrylate based composite electrolyte films in the presence of a lithium salt [25, 80, 92]. Correspondingly, this approach was found to be suitable for the nanopaper reinforced composite electrolytes in Paper IV as well. Transparent, flexible, smooth, and easy-to-handle free-standing films were obtained after curing, Figure 15.



*Figure 15. The cured composite electrolyte product.*

The readily-formed free-standing films were easy to handle, even after post swelling with a liquid electrolyte, and easily mounted in the characterization instruments used.

Success of the curing reaction was also here confirmed using FT-IR, monitoring the disappearance of the peak corresponding to the vinyl bond stretch in the methacrylate group of the oligomers. The FT-IR spectra, Figure 16, shows the absorption of the uncured oligomer mixture (top), sample Ref1

(middle) and sample B1 (bottom) after curing and swelling, verifying full conversion within the detection limit of the FT-IR technique.

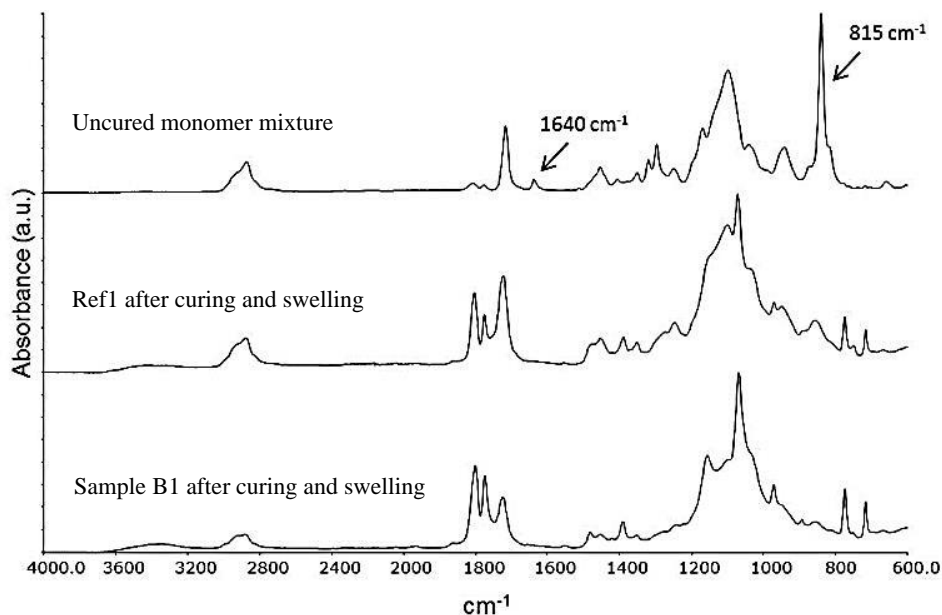


Figure 16. FT-IR spectra of the uncured monomer mixture (top), sample Ref1 (middle) and sample B1 (bottom) after curing and swelling.

### 4.3 Effect of crosslink density on the mechanical properties

All studies showed that the crosslink density has an extensive impact on the mechanical properties of the SPE. It was shown in a tensile test study that although some samples in the series had a high crosslink density and  $T_g$ , they could still exhibit large elongations at break. This can be seen in Figure 17, where sample 1.8 ( $T_g = 92$  °C) has a strain at break at >10%. The crosslink density is by far the parameter that influences most on the mechanical properties. The material goes from displaying a brittle fracture behavior of sample 1.8 to a soft fracture behavior of sample 1.4. However, it can also be seen

that the presence of lithium salt makes the material more capable of handling strain which is clearly illustrated if sample 1.10 and 1.13 are compared, where the former has a salt content of 6% and a strain at break at 20%, whereas the latter with 18 % salt exhibits a failure strain of above 25%. This in spite of both samples having the same crosslink density of the polymer, and it is therefore indicated that the salt is somewhat working as a strengthener of the material, increasing the elongation at break of the SPE. This would be explained by the fact that the lithium cation is coordinating to ether oxygen throughout the structure, thus holding it together at a larger extent.

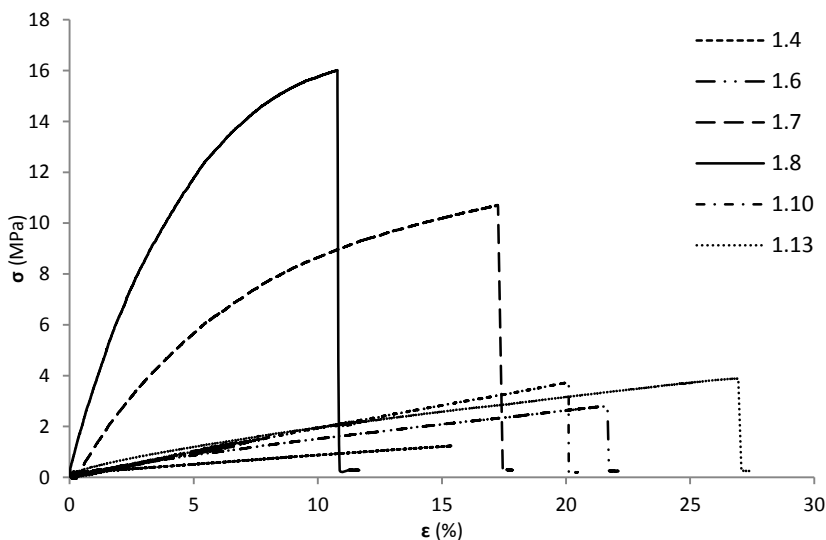


Figure 17. Tensile test curves on some selected samples in Paper I.

When observing the effects on the storage modulus,  $E'$ , it can be seen that a higher crosslink density increases  $E'$  significantly (Figure 18), reaching from a little less than 1 MPa up to 2 GPa.

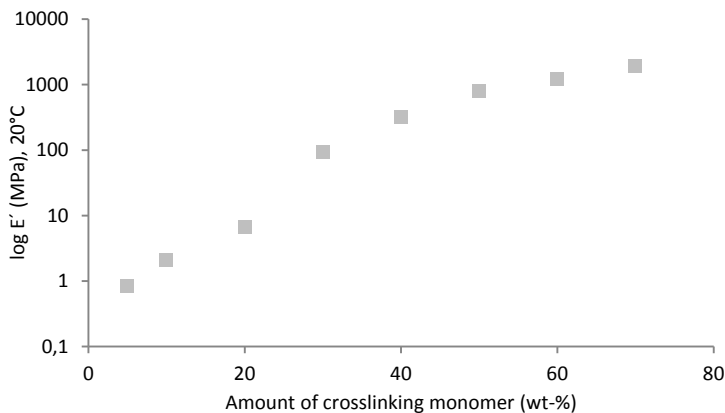


Figure 18.  $E'$  at 20 °C for samples 1.1-1.8.

The storage modulus is also partly affected by the amount of lithium salt added, where it was shown that the modulus and the  $T_g$  increases with increased lithium salt content. This is, as mentioned above, due to the coordination of the lithium to oxygen in the glycol units, and resulting in the formation of occasional “crosslinks” that are formed through the lithium-oxygen interaction. This can be seen in Figure 19, where  $\tan \delta$  is depicted for sample 1.10, 1.6 and 1.13.

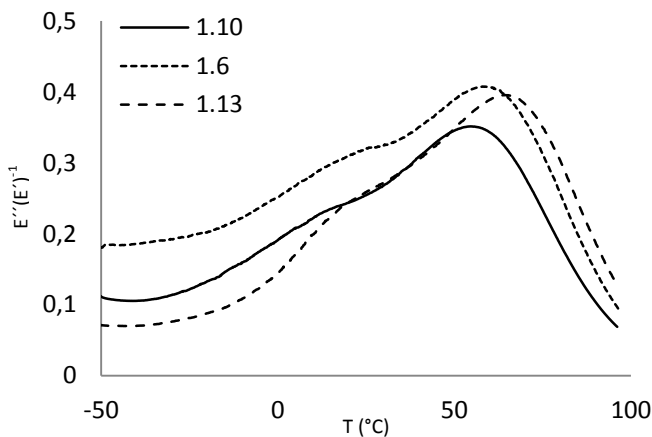


Figure 19.  $\tan \delta$  for samples 1.10, 1.6 and 1.13.

Since the samples 1.10-1.13 had a rather high crosslink density (and a  $T_g$  around 60 °C), it was assumed that the variances in the properties of the material due to the lithium salt content would have been larger if the SPE was more sparsely crosslinked. Therefore, continued studies focused on comparing the influence of lithium salt content on densely crosslinked and sparsely crosslinked systems.

Two series (2.1-2.6 and 2.7-2.12) were manufactured as presented in Table 2. One was above its  $T_g$  at room temperature, and one was below or slightly below its  $T_g$  at room temperature. It was demonstrated that both the  $T_g$  and the modulus was affected more extensively by the lithium salt content when the polymer network was more sparsely crosslinked. This can be seen when comparing the results presented in Figure 20 and 21.

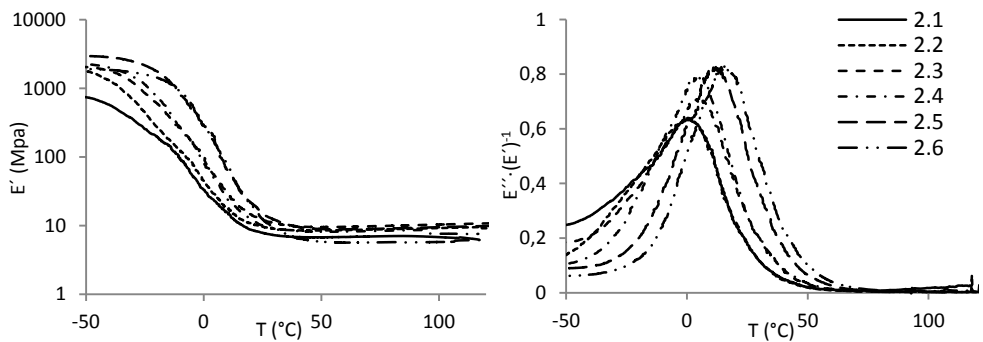


Figure 20. a)  $E'$  (left) and b)  $\tan \delta$  (right) for samples 2.1-2.6.

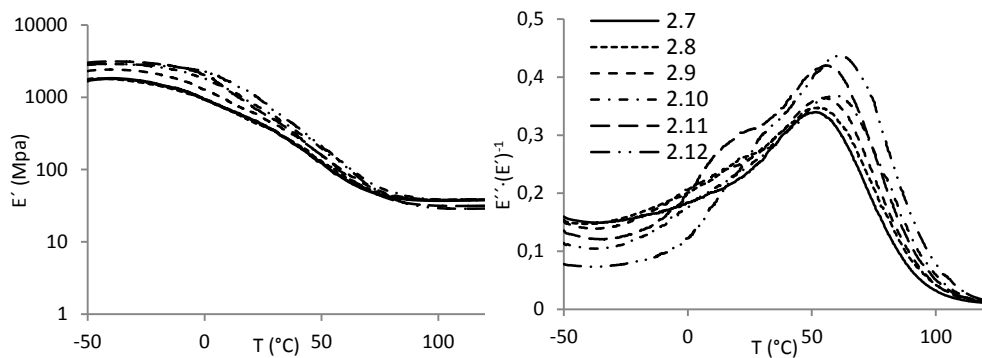


Figure 21. a)  $E'$  (left) and b)  $\tan \delta$  (right) for samples 2.7-2.12.

In accordance to results stated in the previous study described above, it makes sense that the lithium salt content will have a larger impact on the mechanical properties in less crosslinked systems because a minor contributor increasing the effective crosslinking in this system will be more pronounced.

The addition of thio-ethers to the system largely affects the mechanical properties of the electrolyte, as an increased amount of thio-ethers results in a more flexible material (Figure 22a). This is explained both by the decrease in crosslink density but also by the addition of thio-ether segments. The thiol-ene reaction is a step-wise reaction that proceeds through a free radical mechanism, the polymer network will be more homogenous than for SPEs manufactured through free radical methacrylate chemistry only, due to a later gelpoint and a more homogeneous process, which is significant for a step-wise polymerization. This is illustrated in Figure 22b where the  $\tan \delta$  of series 3.1-3.5 is depicted, and it clearly shows that the more thiol compound added, the narrower the glass transition region becomes.

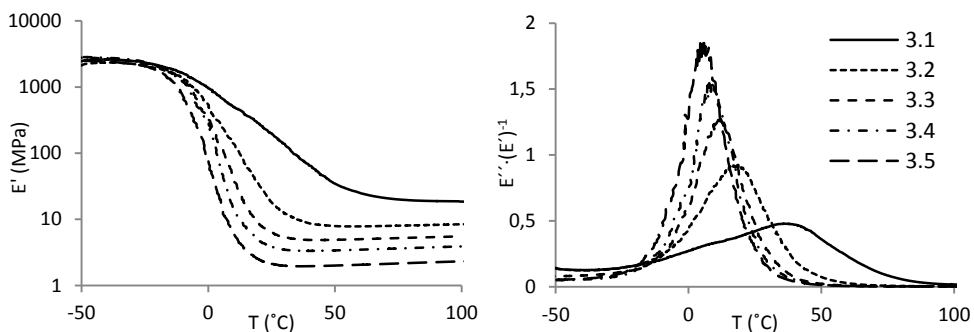


Figure 22. a)  $E'$  (left) and b)  $\tan \delta$  (right) for samples 3.1-3.5.

A more distinct  $T_g$  region might be both advantageous and disadvantageous. It is easier to tune more in detail at which temperature the transition is taking place, thus making the material more well-defined. This suggests that the SPE could be optimized with regards to the glass transition and the ionic conductivity at a given working temperature for the electrolyte. On the other hand, a more homogenous polymer network might be more brittle and incapable to withstand crack propagation throughout the material. However, a more homogenous network on a molecular level would be more beneficial when electrolytes of very small geometries are to be made, since the electrolyte then will hold continuous properties throughout this small geometry.

It should be noted that the thiol-monomer reacting via a coupling reaction may be considered as a three functional monomer whereas the di-methacrylate reacting via a chain wise route is four functional with respect to connectivity. The di-methacrylate however is di-functional in this respect if it reacts with a thiol. Therefore, addition of thiol gives a larger molecular weight between crosslinks,  $\bar{M}_c$ , which is effectively illustrated in Figure 23.  $\bar{M}_c$  is calculated as (eq. [1])

$$\bar{M}_c = \frac{3\rho RT}{E'} \quad [1]$$

where  $\rho$  is the density of the SPE,  $R$  is the ideal gas constant,  $T$  is the temperature and  $E'$  is the storage modulus in the plateau region above the glass transition temperature [93].

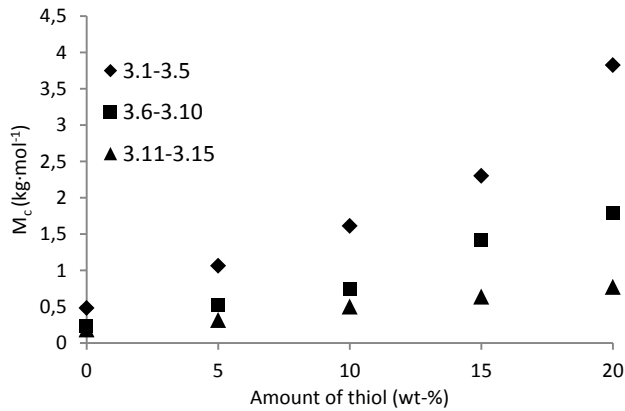


Figure 23. The molecular weight between crosslinks,  $\bar{M}_c$  as a function of thiol compound added.

The results on the mechanical analysis of the composite electrolytes obtained in Paper IV are shown in Figure 24. When looking at the elastic modulus curve for the unreinforced polymer compared to the reinforced counterparts, it is readily seen that the storage modulus is increased significantly when the matrix is reinforced with nanopaper. The modulus increases nearly 600 times compared to the unreinforced polymer, above its  $T_g$ .

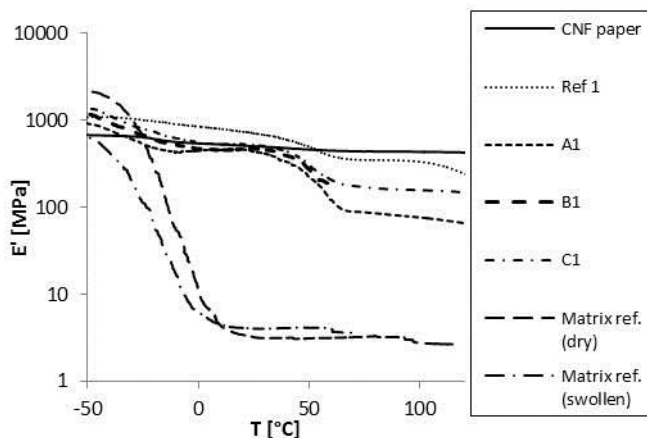


Figure 24.  $E'$  shown for the composites having CNF reinforce with varying amount of acryloyl : propionyl modification, as well as the curves for the neat polymer and CNF nanopaper respectively.

The pure polymer matrix exhibit a low  $T_g$  around  $-20$  °C with a very low modulus in the rubbery state. The pure CNF nanopaper on the other hand exhibits no detectable phase transition and a high modulus throughout the measurement range. The composite materials all exhibit two phase transitions; one low, corresponding to the  $T_g$  of the pure matrix' and one transition around  $50$  °C. This higher transition is proposed to originate from an interphase region in the material i.e. the polymer matrix in close proximity to the fibre surfaces [94]. Comparing the unmodified CNF nanopaper with the modified counterpart it is observed that the unmodified exhibit a higher modulus. This can be explained by stronger interactions between the reinforcing fibres when unmodified.

Sample B1 having a high amount of acrylate modification exhibited a brittle behavior leading to failure around  $60$  °C. A plausible explanation is that a combination of high crosslink density at the fibre surfaces and the post-

swelling with EC:DEC induces stresses at the interface with subsequent loss in ductility.

Furthermore, it can be interpreted from these results that in the sample with the lowest amount of acrylates, relatively poor mechanical performance is obtained compared to the sample with an equal amount of acrylate and propionate groups.

All together the results imply that if the interfacial bonds are too few, the polymer is more mobile and undergoes its glass transition with less restraint of the CNF nanopaper. When the bonds are too many, the composite becomes too brittle. With an equimolar modification (samples C1 and C2) the modified CNF nanopaper composite exhibits an excellent modulus ( $>100$  MPa), even above  $100$  °C, in its swollen state.

#### 4.4 Properties of ionic conductivity

It has clearly been shown that the mechanical properties are widely affected by the crosslink density. This is also the case for the ionic conductivity, which decreases as the  $T_g$  is increased. This is perhaps best seen in Figure 25, where the storage modulus as a function of the crosslink density shown in Figure 18 above is depicted in the graph together with the ionic conductivity of each sample respectively.

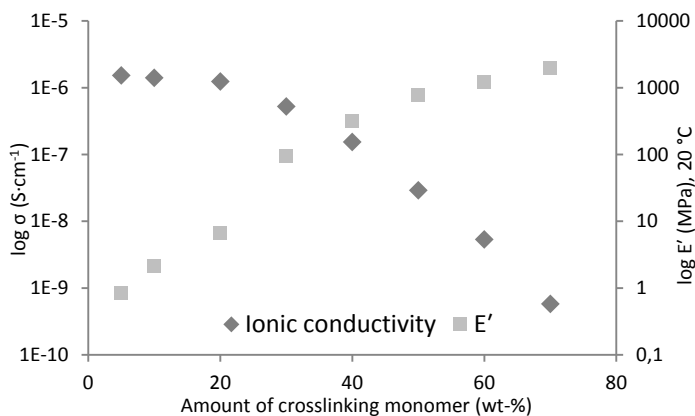


Figure 25. The connected behavior of ionic conductivity and storage modulus for samples 1.1-1.8.

However, there were no significant results on the ionic conductivity due to changes in the salt content, which is presented in Paper I. Also in this case, it was assumed that the changes of the ionic conducting ability would be easier to detect in more sparsely crosslinked systems. This assumption turned out to be false. If considering the effects of lithium salt content on the ionic conductivity (Figure 26), the measurements shows very similar trends with increased salt for both systems (where series 2.1-2.6 is sparsely crosslinked and 2.7-2.12 is more dense), although they are separated by circa 1.5 decades.

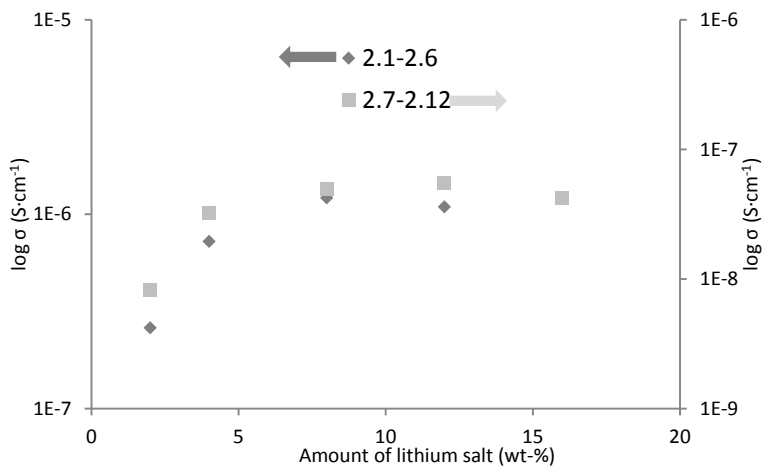


Figure 26. Ionic conductivity of sample 2.1-2.12. The pattern of the conductivity values are about the same, although separated by circa 1.5 decades.

There is a threshold value when around 4 wt-% lithium salt is added, above of which more salt does not contribute to a higher ionic conductivity, and a leveling of the ionic conductivity is observed. It is clear that the crosslink density, and hence the  $T_g$ , is the major affecting parameter on the ionic conductivity. Nonetheless, in loosely crosslinked SPEs, the salt concentration affects the  $T_g$  more than in the highly crosslinked series, and therefore the salt content in sparse systems will be more critical for the ionic conductivity when the SPE is to be used in temperatures around the  $T_g$ .

Another illustration of the important role played by the ability of the molecular chains between the crosslinks to move and be flexible, is emphasized by measurements of the average molecular weight between crosslinks,  $\bar{M}_c$  (Figure 23), contra the ionic conductivity (Figure 27a) and  $T_g$  of the material (Figure 27b).

The ion conducting ability of the electrolyte is affected both by the composition amount of the mono- and di-methacrylated oligomers but also the amount at which the thiol monomer is added. Noteworthy is that the first samples in each sub-series are separated in  $T_g$  by exactly 38 °C (Figure 27b) although studying Figure 27a, the difference in ionic conductivity between the same samples varies about 1 decade between sample 3.1 and 3.6, but more than 2 decades between sample 3.6 and sample 3.11 (which is immeasurable due to too high resistance). This emphasizes the large influence on conductivity given by the mobility of ethylene oxide chain segments.

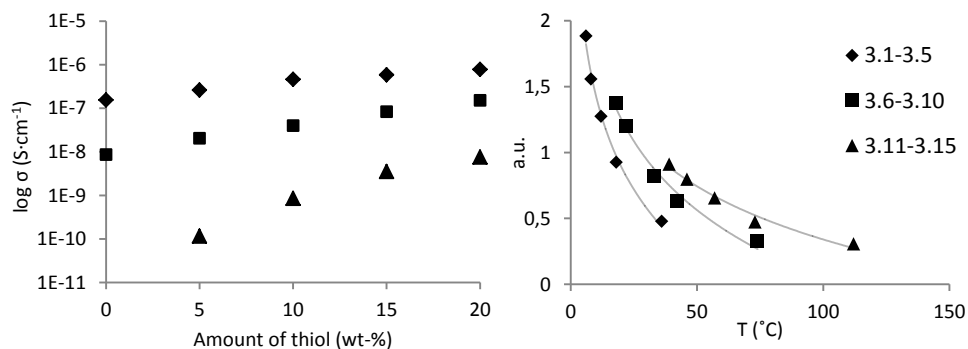


Figure 27. a) The ionic conductivity (left), and b)  $T_g$ s (right) from the  $\tan \delta$  value of samples 3.1-3.15.

The addition of thio-ethers to the system affects the conductivity of the more crosslinked series, series 3.11-3.15, at considerable magnitude. Bearing in mind the results presented in Figure 27a above, it can be seen that the ionic conductivity is increased by over 2 decades when 20 wt-% thiol has been added in series 3.11-3.15, while the storage modulus is shown to drop around 50%. This can be compared to the difference in series 3.1-3.5 and 3.6-3.10, where the conductivity changes with a magnitude of 1 decade, but the modulus at 20 °C decreases more than 95% (see Paper III). This indicates that when the thermoset has a high crosslink density, the crosslink den-

sity is the major controlling factor of the ionic conductivity. At low crosslink densities however, the structure between the crosslinks becomes increasingly important. In other words, if the mesh just gets sparse enough, the crosslink density plays a minor role when it comes to ionic conductivity.

All samples in Paper **IV** were evaluated with electrical impedance spectroscopy, even though the neat polymer matrix samples and the swollen counterparts were too fragile to give trustworthy measurements. The results presented in Figure 28 shows that all composite electrolyte sample exhibits values  $>10^{-5}$  S cm<sup>-1</sup> and all in the same decade. However, it can be noted that the A1 samples having the 1:9 composition (acryloyl chloride : propionyl chloride) have a value of almost a decade higher than the reference samples.

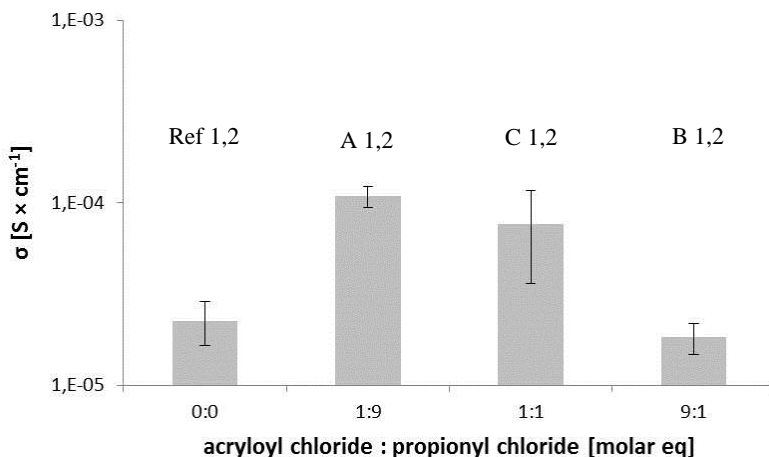


Figure 28. Ionic conductivities for all composite samples prepared in paper **IV** at 25 °C.

The samples having unmodified CNF (Ref 1, 2) measures lower since polymer has left the composite and ionic pathways are obstructed. When considering the samples with a larger amount of acrylate groups the composite loses ionic transporting ability. This is again due to limitations of segmental

motion of the PEO segments, which here are restricted by an increased amount of covalent bonds between the phases. Furthermore, samples Ref1 and 2 show a more moderate ionic conductivity as well indicating a strong fibre / matrix interaction in the solid state.

## 4.5 Electrochemical stability

In an attempt to quantify the influence on the electrochemical stability from having thio-ethers in the structure sweep voltammetry was conducted, Paper III, Figure 29. As mentioned above in the experimental part, samples from least crosslinked series were chosen, since a too high resistance of the more cross-linked counterpart may influence on the measurement. It is evident that both samples show a relatively stable behavior in the anodic sweep region, and they are both quite stable in the region 6 V vs.  $\text{Li}/\text{Li}^+$ . However, the sample containing thio-ethers demonstrate a more critical performance towards the cathode than the sample with pure PEO, especially if graphite is the electrode in question. It should on the other hand be noted that both samples are deviating moderately with respect to the current density.

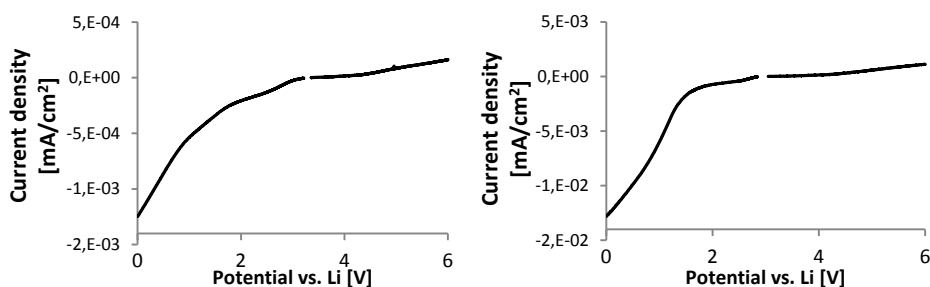
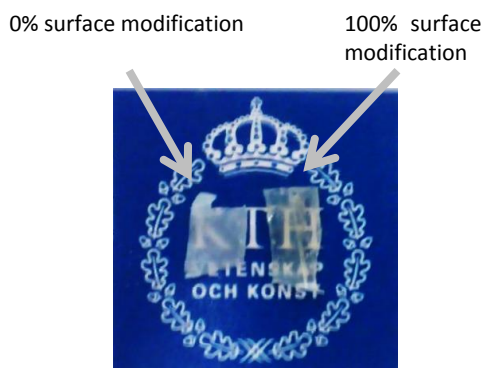


Figure 29. Sweep voltammetry curves for (a) a non-thiol sample, 3.1, and (b) a sample with 20% thiol compound, 3.5.

## 4.6 Swelling tests in EtOH

In order to obtain a reliable confirmation on the degree of success to which the polymer was actually bonded to the CNF in Paper **IV**, swelling tests were conducted. The samples were immersed in EtOH and put on a shaking table for 48 hours. Since EtOH is an excellent solvent for PEO, a larger amount of PEO was expected to migrate from the unmodified CNF nanopaper than from the modified. After 48 hours, the sample with unmodified CNF is turning opaque again, while the sample with modified CNF's retains a higher transparency (Figure 30).



*Figure 30. The composite electrolyte with unmodified CNF nanopaper (left) and modified CNF nanopaper (right) after swelling in EtOH for 48 hours.*

This means that a larger amount of polymer has been removed from the unmodified CNF nanopaper compared to the modified one. This is indicating that the polymer being covalently attached to the CNF in the latter case, and not just embedded as seems to be the case in the unmodified sample. These results furthermore indicate the importance of a strong interface when the material is subjected to swelling stresses.

The possibility of the polymer electrolyte to diffuse out from the system will further be important for the long term performance of the composite electrolyte in a battery application. Furthermore, not only the load bearing ability will be affected but also the electrochemical behavior will deteriorate with increased porosity. Changes in geometry are also imposed in a battery during charging / uncharging cycles why a strong interface is needed.

## 4.7 Composite electrolyte morphology

To investigate the morphology of the composite electrolytes, Paper IV, SEM imaging was conducted. Figure 31 shows representative images of Ref1, A1 and B1. In sample Ref1 the wetting of the oligomer is poor when fractured, which is manifested by segments of naked CNF fibres, uncovered with polymer. On the other hand, if considering image 31b and-c, it can be noted that the polymer is covering the CNF fibres well. This further emphasizes the importance of having a covalent bonding at the interface when the composites are subjected to dimensional changes as will be expected in a working lithium ion battery.

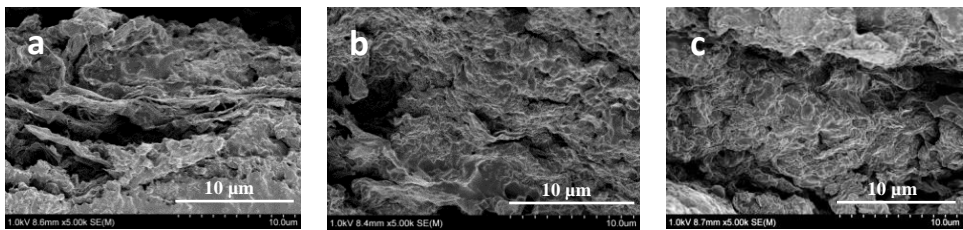


Figure 31. SEM images of sample a) Ref1, b) A1 and c) B1.

## 5. CONCLUSIONS

In Paper **I**, series of solid PEO methacrylate electrolytes were successfully manufactured through UV initiated free radical polymerization, and the advantages of the rapid, robust processing technique demonstrated was stressed. The manufacturing route offers the ability to add the lithium salt in situ and the mixture is subject to low thermal loads upon curing. The electrolytes produced held a broad range of both mechanical as well as ion conducting properties. They were produced in a process where the lithium salt and a photo initiator were dissolved in the monomer mixtures before curing. Furthermore, the mixtures were then irradiated with UV light, initiating radical polymerization to obtain solid, smooth, homogenous ion conducting electrolytes. The storage modulus at 20 °C was found to range from 0.8 MPa to well above 1.5 GPa depending on the monomer composition. The conductive performance started off at fairly good conductivities at  $1.5 \times 10^{-6} \text{ S} \times \text{cm}^{-1}$  and dropped dramatically as the material got stiffer due to a higher crosslink density. These large variations in both mechanical properties as well as electrical conductivity accentuate the versatility of the production technique, but also in the properties and performance of the materials produced.

In the second study presented in Paper **II**, two series of PEO-based thermoset lithium battery electrolytes with varied lithium salt content were studied with respect to its impact of on the mechanical and electrical properties. The thermoset series were alternated with respect to crosslink density and  $T_g$  transition. The less crosslinked system had a  $T_g$  below room temperature and the more crosslinked system had a  $T_g$  above room temperature. Similar trends of an increase in conductivity with increased lithium salt content are seen in both series. The overall levels of conductivity however differed significantly, with a higher level for the low  $T_g$  series. The salt content was also

found to affect the  $T_g$  transition by shifting the  $T_g$  upwards with increasing salt content. This effect was more significant for the low  $T_g$  system with a low crosslink density. The coordination of a lithium salt to the PEO-segments was shown to play an important role for the physical state of the material especially when there was less restriction due to crosslinking of the PEO-chains.

Furthermore, in Paper III, three series of SPEs were successfully manufactured in a solvent-free process utilizing the UV irradiation polymerization technique. The three series were polymer networks of mono-methacrylate(ethylene oxide) and a di-methacrylate(ethylene oxide) in varying amounts, which resulted in thermoset networks with different crosslink density. Furthermore, in four of the samples in each series, a thiol compound was added to the reaction mixture and polymer networks with thio-ether segments incorporated was obtained. The addition of a thiol compound resulted in SPEs with differences in both mechanical and ion conductive properties. One of the series was practically above its  $T_g$  at any thio-ether content, while the systems in the second series were both below and above its  $T_g$  at room temperature depending on how much thiol that was added. The systems in series three were below their  $T_g$  at room temperature regardless of the amount of thiol added within this study. It has been shown that competitive structural electrolytes can be produced this way and with these constituents. Addition of thiol was shown to improve the ion conducting abilities, although it is not clear whether this was only a result of a more flexible material (where ethyleneoxide segments are able to move at a larger extent) or if also the introduction of sulfur to the network was affecting, due to its different coordination strength to the lithium ion. It was also found to be the case, that when a large amount of thiol compound was added to the system, not every thiol group within the thiol monomer reacted with an –ene when the salt was present. This would increase the extent at which free vol-

ume is introduced to the material, hence making ion transport easier. The increase of free volume emphasizes the cautions that need to be taken regarding the amount thiol monomer added to a structural electrolyte, although it was shown that the properties of the SPE were largely affected already at moderate amounts of the thiol monomer. The study presented showed that a thiol compound is compatible with a methacrylate(ethylene oxide) based lithium electrolyte network and initial sweep voltammetry results also showed that thio-ethers are stable enough for the application intended. Besides the conventional possibility to vary the crosslink density, the incorporation of thio-ethers represents yet another tool to find advantageous balances between mechanical- and conductivity properties.

Finally, in Paper **IV**, a series of 4 composite electrolytes was produced. The composite electrolytes are constituted of a soft, ionically conductive polymer matrix having a stiff CNF nanopaper as reinforcement. The reference samples contain unmodified CNF, while the other samples in the series are surface modified by a straightforward reaction to create covalent bonds between the CNF and the polymer matrix to different extents. After swelling the composite electrolytes with liquid electrolyte, the sample with the lowest amount of acrylate modification is the best ionic conductor. However, when both the mechanical properties and ionic conductivity performance is considered, the samples modified by an equimolar solution of propionyl chloride and acryloyl chloride is the best choice, having an elastic modulus  $>100$  MPa above  $100$  °C and a ionic conductivity of around  $5 \times 10^{-5}$  S  $\text{cm}^{-1}$  at  $25$  °C. In conclusion, these promising results presented does by far meet the criteria set up by Snyder et al. and others for structural batteries ( $E' > 150$  MPa,  $\sigma > 1 \times 10^{-5}$  S  $\text{cm}^{-1}$  at room temperature) [35, 91].

## 6. FUTURE WORK

To summarize, these four studies comprise a large part of work to investigate the ability of making both homogeneous polymer electrolytes and two phase electrolytes for structural battery applications. However, these systems are associated with limits on how well they can function as SPEs in structural batteries. Therefore, future work should involve to look into usage of inter penetrating networks (IPNs), where the SPE is reinforced on a molecular level. In an IPN a good conducting linear polymer can be reinforced by a polymer network with high mechanical strength. The network and the linear polymer are not bonded to each other. Finally, an interesting approach could be to form an amphiphilic polymer co-network (APCN) and use it as an electrolyte. In these types of networks two monomers or oligomers are covalently bonded to each other. One of them is a good ionic conductor and one is a mechanical strength provider. As for the work conducted on the CNF reinforced electrolytes, other modification techniques of the cellulose could be interesting to perform as well as studies on the chemical stability through for instance cyclic voltammetry.

## 7. ACKNOWLEDGEMENTS

The Swedish foundation for strategic research (SSF), (grant # RMA08-0002) and the Swedish Energy Agency (grant #37712-1) is greatly acknowledged for financial support to make this research possible.

I would like to take the opportunity to thank professor Mats Johansson, who has been my supervisor during this period of doctoral studies. You have truly been a positive, great support and I admire your ability to always be able to make time for helping me and having interesting scientific discussions, but also private related, even though you are often swamped with work.

Professor Mikael Hedenqvist is acknowledged for co-supervising the project and the input he has contributed with, especially on diffusion. I would also like to thank all my colleagues in the KOMBATT group (Leif, Mats, Göran, Dan, Janis, Mårten, Andrejs, Maria, Eric, Tony) for all great technical discussions and all the fun! Our time in Piteå, the one when we had to go by car back to Stockholm because of the volcano ash cloud kept all planes grounded, was so much fun and a great time to bond.

On that note, Professor Leif Asp is especially thanked for putting together a group with great dynamics and substantial knowledge. Maria H. Kjell and Simon Leijonmarck are specifically acknowledged for all the help with EIS measurements and their patience with me trying to understand some electrochemistry. Eric Jacques is thanked for trying to make me comprehend some fundamental material mechanics, with varying results.

I would like to direct special appreciations to Professor Eva Malmström, who was the one bringing me into the group in the first place. I have really enjoyed collaborating with you. Professor Anders Hult is thanked for all the

great stories from around the world. Robert W is acknowledged for making me understand that I should become a PhD student, for being very calming in critical situations at conferences and so on, and for crashing our room in San Diego. Christian is thanked for being my protégé at the gym, and for being a great friend over these past years. Carl is thanked for always correcting words but also for being a good friend and bringing some food culture into our (in this regard) skimpy group of friends. Yvonne, I would like to thank you for all the fun we've had, for teaching me how to ski and to not doubt myself in any situation. Kim, you have been a true rock and I'm really glad I had the chance to get to know you, and that we were able to go to one last job trip to NoLa together. Sammy P is thanked for all the awesome times in Amherst and for coming to Sweden, and joining in on the brewing. Susanne is thanked all the fun and for being the worst loser ever in the noble game of Gris. Linn is thanked for being so considerate and thoughtful of everybody in the group, and for being a great listener and friend. I also want to thank you for proof reading this thesis. Jan is thanked being the crown princess of MY office. Mauro is thanked for being a great friend with a lot of interesting insights in world politics. Linda is thanked for keeping things in check around here... Kristina is thanked for the nice skiing we did after work the last winter. Susana, thanks for joining the group and give it an energy injection, and for keeping it classy when leaving the bar. Thank you Emelie for these years and for your outstanding collaborations in the "question-of-the-night"-game. Martin is thanked for the nice choir sessions. My deepest thanks and appreciation goes to all my other friends and coworkers, both in the past and the present, at the Division of Coating technology at the Department of Fibre and Polymer Technology, KTH!!!

I would like to give my deepest acknowledgements to my family; Mikael, Ulla-Karin, Johanna, Andreas, Lisa and Frida for supporting me in my studies and being a solid rock to turn to when needed, but also for all nice times we have had together, especially at Blidö.

Last but not least, I would like to express my sincere thankfulness to my dear sweet Helen. Everything changed as you entered my life, mein Schlürpsi. I can't thank you enough for being around, so supportive in the final, critical part of my work. Thank you for all the fun we have had so far and we will have in the future, I really can't wait to spend it with you, and thank you for being you. Love you.

## 8. REFERENCES

1. Matsuki, M., Ozawa, K., *General Concepts*, in *Lithium Ion Rechargeable Batteries*, K. Ozawa, Editor. 2009, WILEY-VCH Verlag GmbH & Co. KGaA, Weinheim. p. 1-9.
2. Megahed, S. and B. Scrosati, *Lithium-ion rechargeable batteries*. J. Power Sources, 1994. **51**(1-2): p. 79-104.
3. Munshi, M.Z.A., B.B. Owens, and S. Nguyen, *Measurement of Li<sup>+</sup> ion transport numbers in poly(ethylene oxide)-LiX complexes*. Polym. J. (Tokyo), 1988. **20**(7): p. 597-602.
4. Xu, K., *Nonaqueous Liquid Electrolytes for Lithium-Based Rechargeable Batteries*. Chem. Rev., 2004. **104**(10): p. 4303-4417.
5. Wetzel, E.D., *Reducing weight: Multifunctional composites integrates power, communications, and structure*. Amptiac Q., 2004. **8**(4): p. 91-95.
6. Shirshova, N., et al., *Structural composite supercapacitors*. Composites, Part A, 2013. **46**: p. 96-107.
7. Lundberg, R.D., F.E. Bailey, and R.W. Callard, *Interactions of inorganic salts with poly(ethylene oxide)*. J. Polym. Sci., Part A-1 Polym. Chem., 1966. **4**(6): p. 1563-77.
8. Fenton, D.E., J.M. Parker, and P.V. Wright, *Complexes of alkali metal ions with poly(ethylene oxide)*. Polymer, 1973. **14**(11): p. 589.
9. Wright, P.V., *Electrical conductivity in ionic complexes of poly(ethylene oxide)*. Br. Polym. J., 1975. **7**(5): p. 319-27.
10. Berthier, C., et al., *Microscopic investigation of ionic conductivity in alkali metal salt-poly(ethylene oxide) adducts*. Solid State Ionics, 1983. **11**(1): p. 91-5.
11. Dupon, R., et al., *Influence of ion pairing on cation transport in the polymer electrolytes formed by poly(ethylene oxide) with sodium tetrafluoroborate and sodium tetrahydroborate*. J. Am. Chem. Soc., 1982. **104**(23): p. 6247-51.
12. Shriver, D.F., et al., *Structure and ion transport in polymer-salt complexes*. Solid State Ionics, 1981. **5**: p. 83-8.
13. Papke, B.L., M.A. Ratner, and D.F. Shriver, *Conformation and ion-transport models for the structure and ionic conductivity in complexes of polyethers with alkali metal salts*. J. Electrochem. Soc., 1982. **129**(8): p. 1694-701.
14. Armand, M., *Polymer solid electrolytes - an overview*. Solid State Ionics, 1983. **9-10**(Pt. 2): p. 745-54.

15. Armand, M.B., M.J. Duclot, and P. Rigaud, *Polymer solid electrolytes: stability domain*. Solid State Ionics, 1981. **3-4**: p. 429-30.
16. Sylla, S., J.Y. Sanchez, and M. Armand, *Electrochemical study of linear and crosslinked POE-based polymer electrolytes*. Electrochim. Acta, 1992. **37(9)**: p. 1699-701.
17. Nagaoka, K., et al., *High ionic conductivity in poly(dimethyl siloxane-co-ethylene oxide) dissolving lithium perchlorate*. J. Polym. Sci., Polym. Lett. Ed., 1984. **22(12)**: p. 659-63.
18. Vincent, C.A., *Ion transport in polymer electrolytes*. Electrochim. Acta, 1995. **40(13-14)**: p. 2035-40.
19. Killis, A., et al., *Dynamic mechanical properties of crosslinked polyurethanes containing sodium tetraphenylborate*. J. Polym. Sci., Polym. Phys. Ed., 1981. **19(7)**: p. 1073-80.
20. Killis, A., et al., *Ionic conductivity of polyether-polyurethane networks containing sodium tetraphenylborate: a free volume analysis*. Makromol. Chem., 1982. **183(11)**: p. 2835-45.
21. Hou, X. and K.S. Siow, *Ionic conductivity and electrochemical characterization of novel interpenetrating polymer network electrolytes*. Solid State Ionics, 2002. **147(3,4)**: p. 391-395.
22. He, D., et al., *Enhanced Ionic Conductivity of Semi-IPN Solid Polymer Electrolytes Based on Star-Shaped Oligo(ethyleneoxy)cyclotriphosphazenes*. Macromolecules 2012. **45(19)**: p. 7931-7938.
23. Meneghetti, P., S. Qutubuddin, and A. Webber, *Synthesis of polymer gel electrolyte with high molecular weight polymethyl methacrylate-clay nanocomposite*. Electrochim. Acta, 2004. **49(27)**: p. 4923-4931.
24. Jankova, K., P. Jannasch, and S. Hvilsted, *Ion conducting solid polymer electrolytes based on polypentafluorostyrene-b-polyether-b-polypentafluorostyrene prepared by atom transfer radical polymerization*. J. Mater. Chem., 2004. **14(19)**: p. 2902-2908.
25. Nair, J.R., et al., *UV-cured polymer electrolyte membranes for Li-cells: Improved mechanical properties by a novel cellulose reinforcement*. Electrochem. Commun., 2009. **11(9)**: p. 1796-1798.
26. Chiappone, A., et al., *Microfibrillated cellulose as reinforcement for Li-ion battery polymer electrolytes with excellent mechanical stability*. J. Power Sources, 2011. **196(23)**: p. 10280-10288.
27. Nair, J.R., et al., *Novel cellulose reinforcement for polymer electrolyte membranes with outstanding mechanical properties*. Electrochim. Acta, 2011. **57**: p. 104-111.

28. Chun, S.-J., et al., *Eco-friendly cellulose nanofiber paper-derived separator membranes featuring tunable nanoporous network channels for lithium-ion batteries*. J. Mater. Chem., 2012. **22**(32): p. 16618-16626.
29. Leijonmarck, S., et al., *Single-paper flexible Li-ion battery cells through a paper-making process based on nano-fibrillated cellulose*. J. Mater. Chem. A, 2013. **1**(15): p. 4671-4677.
30. Peterson, J.J., et al., *Surface-Grafted conjugated polymers for hybrid cellulose materials*. J. Polym. Sci., Part A Polym. Chem., 2011. **49**(14): p. 3004-3013.
31. Scrosati, B. and J. Garche, *Lithium batteries: Status, prospects and future*. J. Power Sources, 2010. **195**(9): p. 2419-2430.
32. Munch Elmer, A., et al., *Ion conductive electrolyte membranes based on co-continuous polymer blends*. J. Mater. Chem., 2003. **13**(9): p. 2168-2176.
33. Liu, P., E. Sherman, and A. Jacobsen, *Design and fabrication of multifunctional structural batteries*. J. Power Sources, 2009. **189**(1): p. 646-650.
34. Thomas, J.P. and M.A. Qidwai, *The design and application of multifunctional structure-battery materials systems*. Jom, 2005. **57**(3): p. 18-24.
35. Snyder, J.F., R.H. Carter, and E.D. Wetzel, *Electrochemical and Mechanical Behavior in Mechanically Robust Solid Polymer Electrolytes for Use in Multifunctional Structural Batteries*. Chem. Mater., 2007. **19**(15): p. 3793-3801.
36. Sperling, L.H., *Cross-linking, Plasticizers, and Fillers*, in *Introduction to Physical Polymer Science*. 1986. p. 14-17.
37. William, D.C.J., *Fundamentals of materials science and engineering*. 2nd ed. 2005: John Wiley & Sons, Inc.
38. Van Krevelen, D.W., *Typology of Polymers*, in *Properties of Polymers*. 1990, Elsevier Science Publishers B.V. p. 7-47.
39. Chanda, M., *Introductory Concepts*, in *Introduction to Polymer Science and Chemistry*. 2006, CRC Press. p. 1-34.
40. Kuo, P.-L., W.-J. Liang, and T.-Y. Chen, *Solid polymer electrolytes V: microstructure and ionic conductivity of epoxide-crosslinked polyether networks doped with LiClO<sub>4</sub>*. Polymer, 2003. **44**(10): p. 2957-2964.
41. Ye, L., et al., *Preparation and evaluation of two kinds of solid polymer electrolytes made from crosslinked poly(ether urethane) elastomers consisting of a comb-like and a hyperbranched polyether*. J. Appl. Polym. Sci., 2008. **109**(3): p. 1955-1961.

42. Chanda, M., *Free Radical Polymerization*, in *Introduction to Polymer Science and Chemistry*. 2006, CRC Press. p. 315-419.
43. Hoyle, C.E., T.Y. Lee, and T. Roper, *Thiol-enes: Chemistry of the past with promise for the future*. J. Polym. Sci., Part A Polym. Chem., 2004. **42**(21): p. 5301-5338.
44. Hoyle, C.E. and C.N. Bowman, *Thiol-Ene Click Chemistry*. Angew. Chem., Int. Ed., 2010. **49**(9): p. 1540-1573.
45. Hoyle, C., et al., *Thiol-enes: fast curing systems with exceptional properties*. RadTech Eur. 05, [Conf. Proc.], 2005. **1**: p. 289-293.
46. Kwisnek, L., et al., *Multifunctional thiols as additives in UV-cured PEG-diacrylate membranes for CO<sub>2</sub> separation*. J. Membr. Sci., 2011. **369**(1-2): p. 429-436.
47. Cramer, N.B., J.P. Scott, and C.N. Bowman, *Photopolymerizations of Thiol-Ene Polymers without Photoinitiators*. Macromolecules, 2002. **35**(14): p. 5361-5365.
48. Åström, B.T., *Introduction*, in *Manufacturing of Polymer Composites*. 1997, Chapman & Hall. p. 1-45.
49. Åström, B.T., *Constituent Material*, in *Manufacturing of Polymer Composites*. 1997, Chapman & Hall. p. 47-135.
50. Hussain, F., et al., *Polymer-matrix nanocomposites, processing, manufacturing, and application: an overview*. J. Compos. Mater., 2006. **40**(17): p. 1511-1575.
51. Okamoto, M., *Nano-clay composites*. Kogyo Zairyo, 2005. **53**(4): p. 52-57.
52. Paul, D.R. and L.M. Robeson, *Polymer nanotechnology: Nanocomposites*. Polymer, 2008. **49**(15): p. 3187-3204.
53. Eichhorn, S.J., et al., *Review: current international research into cellulose nanofibres and nanocomposites*. J. Mater. Sci., 2010. **45**(1): p. 1-33.
54. Klemm, D., et al., *Nanocelluloses: A New Family of Nature-Based Materials*. Angew. Chem., Int. Ed., 2011. **50**(24): p. 5438-5466.
55. Carlmark, A. and E. Malmström Eva, *ATRP grafting from cellulose fibers to create block-copolymer grafts*. Biomacromolecules, 2003. **4**(6): p. 1740-5.
56. Dufresne, A. and M.N. Belgacem, *Cellulose-reinforced composites: from micro-to nanoscale*. Polim. Cienc. Tecnol., 2013. **23**(3): p. 277-286.
57. Missoum, K., M.N. Belgacem, and J. Bras, *Nanofibrillated cellulose surface modification: a review*. Materials, 2013. **6**: p. 1745-1766.
58. Carlmark, A. and E. Malmström, *Atom Transfer Radical Polymerization from Cellulose Fibers at Ambient Temperature*. J. Am. Chem. Soc., 2002. **124**(6): p. 900-901.

59. Malmström, E. and A. Carlmark, *Controlled grafting of cellulose fibers - an outlook beyond paper and cardboard*. Polym. Chem., 2012. 3(7): p. 1702-1713.
60. Bai, W., J. Holbery, and K. Li, *A technique for production of nanocrystalline cellulose with a narrow size distribution*. Cellulose 2009. 16(3): p. 455-465.
61. Goetz, L., et al., *A novel nanocomposite film prepared from crosslinked cellulosic whiskers*. Carbohydr. Polym., 2009. 75(1): p. 85-89.
62. Peng, B.L., et al., *Chemistry and applications of nanocrystalline cellulose and its derivatives: a nanotechnology perspective*. Can. J. Chem. Eng., 2011. 89(5): p. 1191-1206.
63. Lam, E., et al., *Applications of functionalized and nanoparticle-modified nanocrystalline cellulose*. Trends Biotechnol., 2012. 30(5): p. 283-290.
64. Lee, K.-Y., et al., *Bacterial cellulose as source for activated nanosized carbon for electric double layer capacitors*. J. Mater. Sci., 2013. 48(1): p. 367-376.
65. Sturcova, A., G.R. Davies, and S.J. Eichhorn, *Elastic Modulus and Stress-Transfer Properties of Tunicate Cellulose Whiskers*. Biomacromolecules, 2005. 6(2): p. 1055-1061.
66. Iwamoto, S., et al., *Elastic Modulus of Single Cellulose Microfibrils from Tunicate Measured by Atomic Force Microscopy*. Biomacromolecules, 2009. 10(9): p. 2571-2576.
67. Saito, T., et al., *Homogeneous Suspensions of Individualized Microfibrils from TEMPO-Catalyzed Oxidation of Native Cellulose*. Biomacromolecules, 2006. 7(6): p. 1687-1691.
68. Saito, T., et al., *Individualization of Nano-Sized Plant Cellulose Fibrils by Direct Surface Carboxylation Using TEMPO Catalyst under Neutral Conditions*. Biomacromolecules, 2009. 10(7): p. 1992-1996.
69. Horvath, A.E. and T. Lindström, *The influence of colloidal interactions on fiber network strength*. J. Colloid Interface Sci., 2007. 309(2): p. 511-517.
70. Wang, X.J., et al., *Novel composite polymer electrolytes based on poly(ether-urethane) network polymer and modified montmorillonite*. Electrochem. Commun., 2003. 5(12): p. 1025-1029.
71. Liang, W.-J., et al., *Solid polymer electrolytes. XI. Preparation, characterization and ionic conductivity of new plasticized polymer electrolytes based on chemical-covalent polyether-siloxane hybrids*. J. Appl. Polym. Sci., 2006. 100(2): p. 1000-1007.
72. Wu, C.-G., et al., *New solid polymer electrolytes based on PEO/PAN hybrids*. J. Appl. Polym. Sci., 2006. 99(4): p. 1530-1540.

73. Zhou, S. and S. Fang, *High ionic conductivity of all-solid polymer electrolytes based on polyorganophosphazenes*. Eur. Polym. J., 2007. **43**(8): p. 3695-3700.
74. Meyer, W.H., *Polymer electrolytes for lithium-ion batteries*. Adv. Mater. , 1998. **10**(6): p. 439-448.
75. MacFarlane, D.R., et al., *Structure-property relationships in plasticized solid polymer electrolytes*. Electrochim. Acta, 1995. **40**(13-14): p. 2131-6.
76. Zhang, Z.C., et al., *Ion conductive characteristics of cross-linked network polysiloxane-based solid polymer electrolytes*. Solid State Ionics, 2004. **170**(3-4): p. 233-238.
77. Snyder, J.F., E.D. Wetzel, and C.M. Watson, *Improving multifunctional behavior in structural electrolytes through copolymerization of structure- and conductivity-promoting monomers*. Polymer, 2009. **50**(20): p. 4906-4916.
78. Snyder, J.F., M.A. Ratner, and D.F. Shriver, *Optimizing the design of polyelectrolytes by using Monte Carlo simulations*. J. Electrochem. Soc., 2001. **148**(8): p. A858-A863.
79. Kosonen, H., et al., *Mesomorphic Structure of Poly(styrene)-block-poly(4-vinylpyridine) with Oligo(ethylene oxide)sulfonic Acid Side Chains as a Model for Molecularly Reinforced Polymer Electrolyte*. Macromolecules, 2002. **35**(27): p. 10149-10154.
80. Willgert, M., et al., *Photoinduced free radical polymerization of thermoset lithium battery electrolytes*. Eur. Polym. J., 2011. **47**(12): p. 2372-2378.
81. Nair, J.R., et al., *Methacrylic-based solid polymer electrolyte membranes for lithium-based batteries by a rapid UV-curing process*. React. Funct. Polym., 2011. **71**(4): p. 409-416.
82. Decker, C., *Photoinitiated crosslinking polymerization*. Prog. Polym. Sci., 1996. **21**(4): p. 593-650.
83. Decker, C., *New developments in UV radiation curing of protective coatings*. Surf. Coat. Int., Part B, 2005. **88**(B1): p. 9-17.
84. Murray, G.A., J.L. Yates, and S.M. Newman, *Ultraviolet light and ultraviolet light-activated composite resins*. J. Prosthet. Dent., 1981. **46**(2): p. 167-70.
85. Choi, Y., et al., *Ultraviolet radiation curing of acrylates for lithium polymer electrolytes*. J. Appl. Electrochem., 1997. **27**(9): p. 1118-1121.
86. Li, Z., et al., *Novel network polymer electrolytes containing fluorine and sulfonic acid lithium prepared by ultraviolet polymerization*. J. Appl. Polym. Sci., 2008. **108**(4): p. 2509-2514.

87. Vachon, C., et al., *Microphase Separation and Conductivity Behavior of Poly(propylene oxide)-Lithium Salt Electrolytes*. *Macromolecules*, 1995. **28**(16): p. 5585-94.
88. Åström, B.T., *Manufacturing Techniques*, in *Manufacturing of Polymer Composites*. 1997, Chapman & Hall. p. 178-305.
89. Katz, S., R.P. Beatson, and A.M. Scallan, *The determination of strong and weak acidic groups in sulfite pulps*. *Sven. Papperstidn.*, 1984. **87**(6): p. R48-R53.
90. Wågberg, L. and R. Hägglund, *Kinetics of polyelectrolyte adsorption on cellulosic fibers*. *Langmuir*, 2001. **17**(4): p. 1096-1103.
91. Wakihara, M., Nakayama, M. and Kato, Y., *Characterization of Solid Polymer Electrolytes and Fabrication of all Solid-State Lithium Polymer Secondary Batteries*, in *Lithium Ion Rechargeable Batteries*, K. Ozawa, Editor. 2009, WILEY-VCH Verlag GmbH & Co. KGaA, Weinheim. p. 213-251.
92. Willgert, M., et al., *New structural lithium battery electrolytes using thiol-ene chemistry*. *Solid State Ionics*, 2013. **236**: p. 22-29.
93. Chanda, M., *Chain Dimensions, Structures, and Transitional Phenomena*, in *Introduction to Polymer Science and Chemistry*. 2006, CRC Press. p. 37-104.
94. Ståhlberg, D., et al., *Relaxation properties of particle filled coatings: Experimental study and modelling of a screw joint*. *Prog. Org. Coat.*, 2006. **55**(2): p. 112-118.